

Theoretical Studies of Photoinduced Electron Transfer in Dye-Sensitized TiO₂

Walter R. Duncan and Oleg V. Prezhdo

Department of Chemistry, University of Washington, Seattle, Washington 98195;
email: prezhdo@u.washington.edu

Annu. Rev. Phys. Chem. 2007. 58:143–84

First published online as a Review in Advance
on October 23, 2006

The *Annual Review of Physical Chemistry* is
online at <http://physchem.annualreviews.org>

This article's doi:
10.1146/annurev.physchem.58.052306.144054

Copyright © 2007 by Annual Reviews.
All rights reserved

0066-426X/07/0505-0143\$20.00

Key Words

chromophore-semiconductor interface, photovoltaic cell, ultrafast electron injection, electron-phonon interaction, time-dependent density-functional theory, quantum system-bath models, nonadiabatic molecular dynamics

Abstract

This review describes recent research into the properties of the chromophore-TiO₂ interface that forms the basis for photoinduced charge separation in dye-sensitized semiconductor solar cells. It focuses particularly on an atomistic picture of the electron-injection dynamics. The interface offers an excellent case study, pertinent as well to a variety of other photovoltaic systems, photo- and electrochemistry, molecular electronics, analytical detection, photography, and quantum confinement devices. The differences between chemists' and physicists' models for describing molecules and bulk materials, respectively, create challenges for the characterization of interfaces that include both of these components. We give an overall picture of the interface by starting with a description of the properties of the chromophores and semiconductor separately, and then by discussing the coupled system, including the chromophore-semiconductor binding, electronic structure, and electron-injection dynamics. Explicit time-dependent modeling is particularly valuable for an understanding of the ultrafast electron injection because it shows a variety of individual injection events with well-defined dynamical features that cannot be made apparent by an average reaction-rate description.

ET: electron transfer

CB: conduction band

1. INTRODUCTION

Over the past several decades, researchers have investigated the movement of charge through individual molecules, as well as through solid-state structures, and have successfully described them both theoretically. In contrast, the transfer across molecular/bulk interfaces has gained attention only recently and is poorly understood. These interfaces play a key role in many emerging fields, creating a need for a better theoretical treatment of the interfacial electron transfer (ET). Charge transport across the contacts remains the most important area of study in the burgeoning area of molecular electronics (1–7); photoinduced ET at molecular/bulk interfaces constitutes a major focus of research in the chemistry of photoelectrolysis (8), photocatalysis (9–12), and color photography (13); and molecular/bulk interfacial ET is the primary step in many solar energy-conversion devices because it creates free-charge carriers on the absorption of a photon. Increased concerns with energy sources have prompted researchers to propose and test a great variety of these novel photovoltaic designs. Examples include dye-sensitized semiconductor solar cells (14–18), assemblies of inorganic semiconductors with conjugated polymers (19–24), as well as devices employing quantum dots (25, 26), fullerenes (27, 28), and carbon nanotubes (28, 29).

A dye coupled to TiO_2 is an excellent model for processes that occur in the above fields. This system represents one of the best-studied photovoltaic devices, the dye-sensitized semiconductor solar cell, or Grätzel cell. Solar cells of the Grätzel type are based on transition-metal or organic dye molecules that are adsorbed to a highly porous nanocrystalline TiO_2 (14–18). Visible light excites the dye-sensitizer molecules from the ground state, which is located energetically in the semiconductor band gap, to an excited state resonant with the TiO_2 conduction band (CB) (**Figure 1**). The electron is then transferred to the semiconductor on an ultrafast timescale. It travels through the semiconductor to one of the electrodes, carries a load while making its way to the other electrode, and then enters an electrolyte that brings it back to the chromophore ground state.

1.1. Experimental Studies of the Electron Injection

Many experimentalists have investigated the ET dynamics in dye- TiO_2 systems. After developing synthetic methods and characterizing the interfaces (30), they have employed time-resolved laser spectroscopies to monitor the electron injection in real time (17, 31–60). Both the chromophore and the semiconductor electronic states in these studies are accessible by spectroscopic techniques.

Willig's group (38–45) carried out one of the first studies of the interfacial ET and raised important questions about the injection mechanism. Femtosecond laser spectroscopy of the ET between modified perylene chromophores and TiO_2 indicated that the coherent wave packet created in the donor molecule by the pump pulse survived the ET and could be detected in the cation by the probe pulse. This observation conflicted with the usual model of ET, which assumes the reaction starts from a thermally equilibrated occupation of the vibrational modes in the donor, and motivated real-time theoretical studies of the injection dynamics. In addition to monitoring the

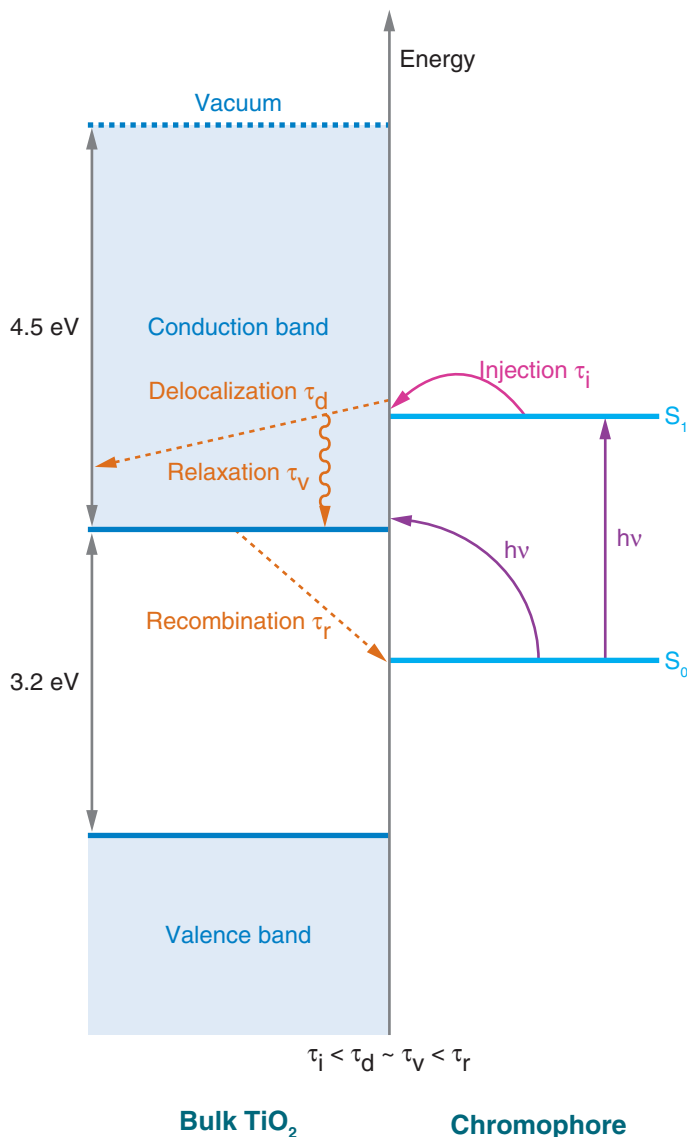


Figure 1

Energy diagram of the chromophore- TiO_2 interface. An absorbed photon promotes an electron from the ground state (S_0) of the dye located in the semiconductor energy gap into an excited state (S_1) that is in resonance with the conduction band (CB). Typically, the dye excited state is well inside the CB. An additional direct photoexcitation from the dye ground state into a semiconductor state near the CB edge becomes possible with a strong coupling as in the catechol- TiO_2 system. In some systems, such as alizarin-sensitized TiO_2 , the dye excited state is located near the edge of the TiO_2 CB. Efficient electron injection into the edge of the CB avoids the energy and voltage loss by relaxation to the CB edge that is inevitable if injection occurs deep into the CB. The injected electron delocalizes from surface to bulk, simultaneously relaxing to the bottom of the CB owing to coupling to vibrations. If the electron returns to or remains trapped at the surface, it recombines with the positive charge residing on either the chromophore or the electrolyte mediator.

perylene chromophores, Willig and coworkers (39) probed the intraband absorption of the injected electrons and found that the rise in the injected electron signal was identical to the rise in the donor cation signal. This combination of experiments demonstrated that on leaving the dye, the electron was not trapped on the surface and indeed entered bulk TiO_2 .

Lian and coworkers (17, 46–57) performed comprehensive and detailed investigations of the ET from different ruthenium (Ru) dyes to TiO_2 by monitoring infrared (IR) absorption of electrons in the semiconductor CB. They found that the injection

Nonadiabatic (NA):

processes that involve transitions between electronic states when chromophore-semiconductor coupling is weak; in contrast, adiabatic processes occur with strong chromophore-semiconductor coupling and involve a single electronic state

Quantum-classical

approaches: separate chemical systems into light/fast and heavy/slow components and treat them using quantum and classical mechanics, respectively

dynamics were biphasic, with an ultrafast component under 100 fs that arises as a result of injection from a nonthermalized excited state and a slower component that corresponds to injection from a relaxed excited state. The ratio of the magnitudes of the two types of transfer was dependent on the ratio of the rate constants of injection from the nonthermalized state and of relaxation to the thermalized excited state. They found the slow component depends on excitation wavelength, dye energetics, the pH of the solution, and the solvent.

Wachtveitl, Grätzel, and coworkers (58, 59) observed the changing absorption spectra of alizarin on TiO₂ using transient absorption spectroscopy. The electron injection and cation radical formation took place on an unprecedented, record 6-fs timescale. This is among the fastest charge-separation reactions reported and studied in real time. The ultrafast injection time recorded in the alizarin-TiO₂ system is not unique among photoinduced interfacial ET events, however. Many other systems exhibit timescales on the order of tens or hundreds of femtoseconds. Schnadt and coworkers (60) deduced an even faster, 3-fs injection time for bi-isonicotinic acid on TiO₂ by measuring the line width using resonant photoemission spectroscopy.

1.2. Theoretical Modeling of the Electron-Transfer Dynamics

Lian, Willig, and other authors (34, 38, 39, 47–50) discuss the origin of the efficient interfacial electron injection and question whether the observed fast injection is mediated by a strong coupling between the chromophore and the semiconductor, leading to an adiabatic ET, or whether a strong coupling is unnecessary as a large density of TiO₂ acceptor states can still give rise to an ultrafast injection time even when the coupling is weak, leading to nonadiabatic (NA) ET. A detailed atomistic simulation of the ET processes in real time can provide direct answers to these questions. The photoinduced electron injection across the chromophore-TiO₂ interface occurs on the ultrafast timescale, typically faster than thermalization processes. Reaction-rate theories have limited applicability in such cases, and the explicit time-resolved details of the injection become essential for a comprehensive understanding.

Researchers perform real-time modeling of the interfacial ET using one of two strategies, as stipulated by computational expense and complexity. The first is a fully quantum-mechanical description of the electronic and vibrational dynamics involved in the ET, which is achieved using simplified models of the interface (40, 42, 61–65). The second strategy is an explicit atomistic treatment of the interface combined with quantum-classical or semiclassical electron-vibrational dynamics, in which the electronic degrees of freedom are described quantum-mechanically by many-body electronic-structure theory, while vibrations are considered using classical or semiclassical mechanics (66–75). The separation of electronic and nuclear masses and timescales justifies the quantum-classical approximation. The two approaches complement each other; simplified models of the interface are constructed in reference to realistic all-atom calculations, and quantum-classical dynamics approaches are tested against fully quantum-mechanical dynamics. Quantum-mechanical models of the interface provide exact dynamics, transparent interpretations of the parameters entering the model, and the ability to vary these parameters to probe and characterize

various injection regimes. Fully atomistic descriptions, conversely, approach the actual interface as closely as possible. They take into account the chemical structure of chromophores, chromophore-semiconductor binding details, and conditions of the surface, giving rise to a spatial-temporal picture of ET with explicit electron and nuclear motions, conformational and chemical changes, and disorder.

Here we review the theoretical work devoted to understanding ET from a variety of chromophores across the TiO_2 surface. Following a brief description of the TiO_2 surface and the types of sensitizer chromophores and chromophore-semiconductor binding, the discussion focuses on the electronic structure and spectra of the chromophore-sensitized TiO_2 surface, and the electron-injection dynamics across the chromophore-semiconductor interface.

2. THE CHROMOPHORES AND THE SURFACES

The properties of the individual constituents that form the dye-sensitized photovoltaic cell are relatively well understood, although they are discussed in different communities that use different terminologies (76, 77). Chemists concern themselves with dyes, physicists with semiconductors. The chromophores are chosen to actively harvest the visible light that penetrates through the ozone layer and reaches the surface of Earth. They should bind to TiO_2 , match the semiconductor energy levels, and be photochemically and thermally stable. TiO_2 has a long history in photoelectrochemistry (78) and is a cheap and robust oxide, in contrast to the more expensive and delicate pure silicon commonly used in current solar cells. TiO_2 can be made highly porous to expose a large surface area for chromophore binding.

2.1. TiO_2 Surfaces

With few exceptions, the majority of the experimental studies on the interfacial ET in the dye-sensitized TiO_2 systems are carried out with TiO_2 particles that are a mixture of the rutile and anatase crystal forms of TiO_2 with a variety of exposed surfaces (79). Rutile 110 is the most stable and best-studied surface (**Supplemental Figure 1**; follow the Supplemental Material link from the Annual Reviews home page at <http://www.annualreviews.org>). Although it has a well-described general surface structure, several different kinds of defects can complicate a complete depiction. These defects include step edges, oxygen vacancies created by annealing, line defects, and impurities. Variations in the structure can significantly affect the chemistry of reactions that occur at the rutile 110 surface. Even describing the ideal surface structure is problematic. In particular, the interaction of rutile 110 with water, which provides a termination layer both in solution and in air, is complex and has been a subject of debate (80, 81).

Rutile 100 has been the subject of less investigation, but it has several advantages when used in theoretical calculations. The interaction of water with rutile 100 is straightforward, and a general form of the stable surface termination can be easily established. In a simulation, the 100 surface allows for a smaller cell, which simplifies the studies. Rutile 001 has a relatively high energy compared with 110 and 100 (79).

VB: valence band

Schottky barrier: occurs owing to charging of the interface

Many experimental studies use colloidal TiO₂ particles that are prepared by the hydrolysis of TiCl₄ in cold water (82). Such colloids have a high anatase content. Anatase surfaces are less well understood because they are harder to investigate experimentally: Large pure anatase crystals are more difficult to obtain than their rutile counterparts. At less than a critical size on the nanometer scale, TiO₂ crystals are often found in the anatase structure because of its lower surface energy relative to rutile. Above the critical size, a mixture of anatase and rutile particles can be converted to pure rutile by heating (79). The great variety of TiO₂ structures, surfaces, impurities, and defects creates significant challenges in theoretical studies. One would like to presume that the results obtained for one surface are characteristic of the entire class of interfacial electron-injection reactions.

The TiO₂ valence band (VB) is formed by oxygen orbitals. The CB of TiO₂ is created by the *d*-orbitals of the titanium atoms. The gap between the valence and CBs of bulk TiO₂ is 3.2 eV, with the CB starting close to the redox potential of the normal hydrogen electrode and approximately 4.5 eV below the vacuum level (78). The presence of a surface induces substantial changes in the electronic structure of the bulk (83). Localized surface states appear both within the bands and in the gap. The dangling bonds of an unsaturated surface introduce multiple states that lower the gap energy to a few tenths of an electron volt. Surface reconstruction and healing reopen the gap. Saturation of the surface with dissociated water or other chemically bonded species brings the gap close to the bulk value. The energies of most surface states that exist in this case lie within the bands. As an *n*-type semiconductor, TiO₂ creates a negatively charged surface region when in contact with air, liquid, or metal by trapping electrons at the surface. To preserve electrical neutrality, a positive charge layer develops just within the semiconductor, causing a shift in electrostatic potential and a bending of band energies upward in the region near the surface. An accumulation of positive charge carriers at the surface moves the bands down. This is possible, for instance, in solutions with low pH. The accumulation of charge at the interface can also create a Schottky barrier to the electron injection. The surface charging effects are significantly decreased when the surface is chemically terminated.

2.2. Sensitizer Chromophores

The chromophores used in the chromophore-sensitized TiO₂ photovoltaic cell harvest visible light and are selected to match the semiconductor energy levels and to be photochemically and thermally stable (84). They fall into two broad categories (**Supplemental Figure 2**): (*a*) purely organic conjugated molecules, such as catechol, alizarin, and perylene, and (*b*) transition-metal/ligand complexes, such as Ru(dcbpy)₂(NCS)₂. The latter, also known as the N3 dye, has emerged as the paradigm of a heterogeneous charge-transfer sensitizer for mesoporous solar cells owing to its high efficiency and photochemical stability (85). The photoactive ligands in the transition-metal-based chromophores are also organic conjugated molecules; however, they are significantly smaller than the purely organic chromophores. The photoexcited states, which are the donor states in the interfacial ET, are similar in both chromophore types and are formed by the π^* -orbitals of the conjugated systems. The

ground state of the purely organic chromophores is also a π -state, but the ground state of the transition-metal-based chromophores is localized on the n -orbitals occupied by the metal's undivided electron pairs.

The purely organic chromophores contain large π -conjugated systems that create small π - π^* energy gaps within the visible spectrum. The energy gap in the transition-metal-based chromophores is determined by the n - π^* energy difference and can be tuned regardless of the π - π^* splitting, which depends on the extent of the π -electron system. Therefore, the ligands attached to the transition metal are relatively small. The π -conjugated system of the purely organic chromophores can be made smaller by including oxygens within the conjugated system. The oxygens lower the excited-state energy owing to a stronger electron affinity relative to the carbons (compare alizarin and perylene in **Supplemental Figure 2**). Small π -chromophores such as catechol are used to sensitize TiO_2 . However, the visible spectral band in such cases relies on strong chromophore-semiconductor coupling and involves a direct transition from the π -ground state into the TiO_2 CB, bypassing the π^* -excited state, which is high in energy (**Figure 1**).

The relatively minor differences in the photoexcited states of the organic and transition-metal chromophores result from the larger excited-state delocalization in the purely organic chromophores, as well as from the positive charge on the transition metal that slows down the transfer of the electron into the semiconductor. Additional complications with the transition-metal chromophores arise from the strong spin-orbit coupling induced by the metal, providing a high probability of intersystem crossing from the photoexcited singlet into a lower energy triplet state. In the cases in which the triplet state lies below the semiconductor CB, the intersystem crossing substantially slows down the ET rate (53).

2.3. Chromophore Binding to TiO_2

The rates and yields of the ET reactions are determined by the energies of the chromophore and semiconductor donor-acceptor states and by the couplings between these states (86). Although the energy levels of the isolated species are typically well-known from both experimental and theoretical work, the coupling can be measured only indirectly and is quite sensitive to the type of computational method. The binding mode (e.g., chemisorption versus physisorption), the relative orientations of the fragments, the perturbations of the chromophore, and the surface geometric and electronic structures that result from binding can all strongly change the strength and extent of the donor-acceptor interaction.

The chromophores are typically bound to the TiO_2 surface with oxygen-containing substituents, such as hydroxy, carboxy, and phosphoric acid groups. Binding via the hydroxy group results in a very strong chromophore-semiconductor coupling because only a single oxygen atom separates the chromophores from the semiconductor. The coupling decreases with carboxyl binding, and it decreases even further with binding through the phosphoric acid group. In many instances, additional bridging groups are present, most typically $(\text{CH})_n$ and $(\text{CH}_2)_n$, to slow down ET from TiO_2 back to the chromophore (87), to enhance surface binding, and to improve

Singlet: a state with zero total spin

Triplet: a state with total spin equal to one

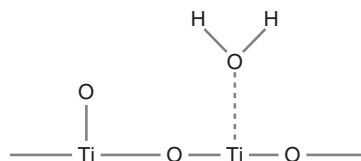
chromophore stability. $(\text{CH})_n$ preserves the chromophore-semiconductor coupling because it simply extends the conjugated π -electron system of the chromophore. $(\text{CH}_2)_n$ significantly decreases the coupling by breaking the conjugation.

Detailed theoretical studies of the binding of sensitizers to TiO_2 have been carried out for relatively few small molecules, revealing the key binding modes that can be expected with the larger species (**Figure 2**). The binding energies, the exact chemistry taking place at the interface, and other details, however, are quite sensitive to theoretical approximations and experimental conditions. In general, for a fixed number of binding groups, larger chromophores lead to increased steric hindrance in certain binding modes, resulting in less variation and sensitivity.

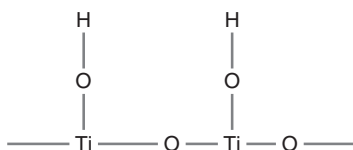
Water on TiO_2 . The adsorption of water is one of the most crucial interactions to understand; ET reactions are often carried out in solution, and there are even significant amounts of water in ultrahigh vacuum experiments. Because the semiconductor surfaces have a substantial number of defects, it is important to understand how water binds both on the perfect surfaces and at defect sites. Representative examples of theoretical work on the binding of water to rutile TiO_2 surfaces (79–81, 88–91) highlight the problems encountered in such work and give general conclusions. The absorption of water on anatase surfaces has been studied far less (92).

Both molecular and dissociative adsorption of water on TiO_2 are possible, depending on the surface and water coverage. Most research supports the idea that rutile 100 encourages dissociation at low surface coverages and is followed by molecular adsorption as the coverage level increases (79). Some simulations predict only molecular adsorption for the defect-free surface (88). The case with rutile 110 is less clear and strongly condition dependent (80, 81, 88–91). Even though experimental work tends to support the dissociative binding at defect sites, the temperature at which the water dissociates is still debated (79). Theoretical studies predict both dissociative and molecular adsorption (**Figure 2**). Although surface defects favor the dissociative mechanism, hydrogen bonding to other physisorbed water molecules stabilizes molecular adsorption. In the absence of efficient hydrogen bonding or other specific interactions, larger molecules containing hydroxyl groups, such as alcohol solvents or sensitizer chromophores, can be expected to adsorb dissociatively.

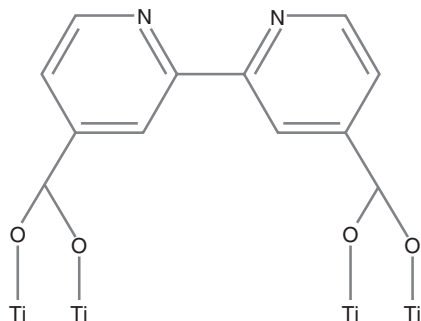
Formic acid on rutile 110 and anatase 101. The adsorption of carboxylic acids is particularly relevant to understanding the dye- TiO_2 interface because many chromophores are attached to the semiconductor via the carboxylic group. The small formic acid molecule represents the binding of many other, significantly larger carboxylic acids. Both theoretical and experimental work have shown that HCOOH generally dissociates at rutile surfaces with the proton transferred to a lattice oxygen (79, 93, 94). Two different modes of dissociative adsorption are possible. In acidic dissociation, the OH bond is cleaved, which results in a formate ion and a proton. The basic cleavage involves the breaking of the CO bond and the formation of HCO^+ and OH^- . Even though the basic dissociation is more likely in the gas phase, the acidic dissociation is much more favorable on the TiO_2 surface owing to the strong



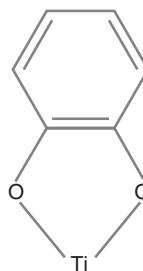
Molecular adsorption of water on rutile 110



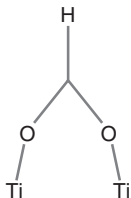
Dissociative adsorption of water on rutile 110



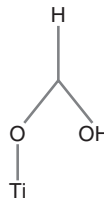
Bi-isonicotinic acid adsorption on rutile 110 and anatase 101



Bidentate adsorption of catechol on a defect site of anatase 101



2-M-bidentate dissociative formic acid adsorption on rutile 110 and formate on anatase 101



Monodentate molecular adsorption of formic acid on anatase 101

Figure 2

Key chromophore-TiO₂ and water-TiO₂ binding motifs. Dissociative adsorption is typically more thermodynamically favorable than molecular adsorption because it saturates a larger number of surface dangling bonds. Chromophores can bind through either one (monodentate) or two (bidentate) bonds to the same surface atom, depending on the match between chromophore and surface geometries.

bidentate bridging between the resulting formate ion and the semiconductor surface (93). The binding energy for the formic acid is significantly larger than that of water. In structures with defects, formate (unlike water) binds asymmetrically to the Ti³⁺ site with a weaker interaction between the formate oxygen and a neighboring Ti⁴⁺ site (94).

Density-functional theory (DFT): an approach to many-body electronic structure theory based on electron density rather than wavefunction

Theoretical studies of anatase 101 have predicted that the most stable binding mode on a dry surface is molecular monodentate (**Figure 2**). The presence of water, however, promotes formic acid dissociation (95). The bidentate bridging configuration is a more stable form for dissociative binding than the monodentate configuration. The formate ion creates a bidentate bridging structure both on wet and dry surfaces. On the hydrated anatase 101 surface, HCOOH and HCOONa form an inner sphere adsorption complex, staying inside the first water layer and attaching directly to the surface.

Catechol on anatase 101. The catechol molecule is one of the smallest sensitizer chromophores and provides two hydroxyl groups for binding to the semiconductor (**Figure 2**). The binding patterns seen with catechol are also characteristic of the larger alizarin (**Supplemental Figure 2**) and coumarin, which, as with catechol, have been the focus of recent time-resolved experimental and theoretical studies (51, 54, 58, 59, 66, 67, 71–75, 92, 96–98). Ab initio molecular orbital theory (99) and density-functional theory (DFT) (100) simulations of catechol adsorption on the anatase 101 TiO₂ surface (92) indicate that the molecular adsorption is more favorable on the perfect 101 surface than is the dissociative mechanism. When the nanoparticles were allowed to relax in the region surrounding the adsorption site, however, the two mechanisms gave similar reaction energies. Researchers also found different results for relaxed and unrelaxed bridging structures. In unrelaxed structures, there were no bridging configurations because the structures were too strained. In the relaxed structures, however, the dissociative bidentate configuration had the same degree of stability as did the monodentate and molecular mechanisms. The most stable configuration was the dissociative addition at the Ti=O defect site. Here the catechol was able to form two relatively strong bonds to a single surface Ti. A significant amount of charge was transferred from the Ti to the catechol on binding.

Bi-isonicotinic acid on rutile 110 and anatase 101. Bi-isonicotinic acid (60, 68, 69, 101–106) is a ligand in many organometallic dyes that are used in Grätzel cells. It can form up to four chemical bonds with the surface (**Figure 2**). Semiempirical calculations on bi-isonicotinic acid adsorbed to the rutile 110 surface (103) considered five different geometries: three bidentate and two monodentate. The most stable structure had a twist around the molecular axis with the pyridine rings tilted in opposite directions. The structure was only slightly distorted in the area where a central metal atom would attach, showing that the results were relevant for the actual dyes. Ab initio DFT study of adsorption of bi-isonicotinic acid on rutile 110 (102) confirmed that the most stable structure was a bidentate bridge with a large twist between the isonicotinic acid groups. The hydrogens were located on twofold coordinated oxygen atoms, making these oxygens move away from the surface. Comparing the adsorption energy of two isonicotinic acids with that of a single bi-isonicotinic acid, the authors found there was a 40% destabilization that resulted from the adsorbate strain in the second structure.

The periodic semiempirical calculations of bi-isonicotinic acid on anatase 101 (101) considered three different geometries: a one-metal ester bond, a one-metal

bidentate configuration, and a two-metal bidentate bridging mode. In all three cases the dissociated bi-isonicotinic acid protons were bound to the surface oxygens. As with the calculations on the rutile 110 surface (102, 103), the favored binding geometry with anatase 101 was a bridge configuration with a twisted ring geometry in the bi-isonicotinic acid.

3. ELECTRONIC STRUCTURE OF DYE-SENSITIZED TiO₂

The photoinduced ET across the dye-semiconductor interface is governed by the electronic properties of the interface, as well as the electron-phonon interactions. The electronic properties include the alignment of the chromophore and semiconductor energy levels, the electronic coupling between the chromophore and semiconductor states, and the spatial localization of the states, particularly of the acceptor states, which can be either localized surface states or delocalized bulk states. The electron-phonon interactions constitute another type of coupling that is responsible for the electronic energy relaxation and heating and also provides an alternative, NA mechanism for the ET. In this section, we consider the electronic structure of the static interface with frozen phonons. Because of the electronic complexity and size of the transition-metal-based dyes, the interfaces involving smaller organic chromophores have been studied more extensively and are better understood.

3.1. Direct Optical Charge Transfer in Catechol-Sensitized TiO₂

Catechol is one of the smallest chromophores studied in a dye/semiconductor system. The catechol/TiO₂ interface exhibits many interesting features in both its electronic structure and its ET dynamics. Functionalization of the semiconductor surface with catechol causes a strong red shift in the spectrum (54). A new band appears at 420 nm, which is unexpected, given that the lowest energy band in free catechol occurs at less than 300 nm (**Figure 3**). Calculations (66, 74, 92, 96, 98) established that the new band originated as a result of a strong electronic interaction between catechol and TiO₂ and a direct charge transfer from catechol to the semiconductor surface that took place during the photoexcitation. Catechol added a ground-state π -orbital slightly above the VB edge (**Supplemental Figure 3**). The catechol π -orbital became the highest occupied molecular orbital (HOMO) of the combined system (**Figure 4**). A transition between this dye orbital and energy levels with strong contributions from Ti(3d) atomic orbitals near the point of attachment was a strong contributor to the new low-energy band. The accepting orbitals near the CB edge, including the lowest unoccupied molecular orbital (LUMO), had no contribution from the catechol, so the charge transfer was complete. The first orbitals with substantial catechol character in the CB appeared approximately 3 eV above the band edge (**Supplemental Figure 3**). The density of states (DOS) was near its maximum at this point, and the dye excited state π^* -orbital, therefore, had a large number of states with which to interact. The highest level of catechol contribution to the individual orbitals in this region was less than 25%, indicating that even photoexcitation at the energy of the first excited state of the isolated molecules would shift the electron density onto the semiconductor.

HOMO: highest occupied molecular orbital

LUMO: lowest unoccupied molecular orbital

DOS: density of states

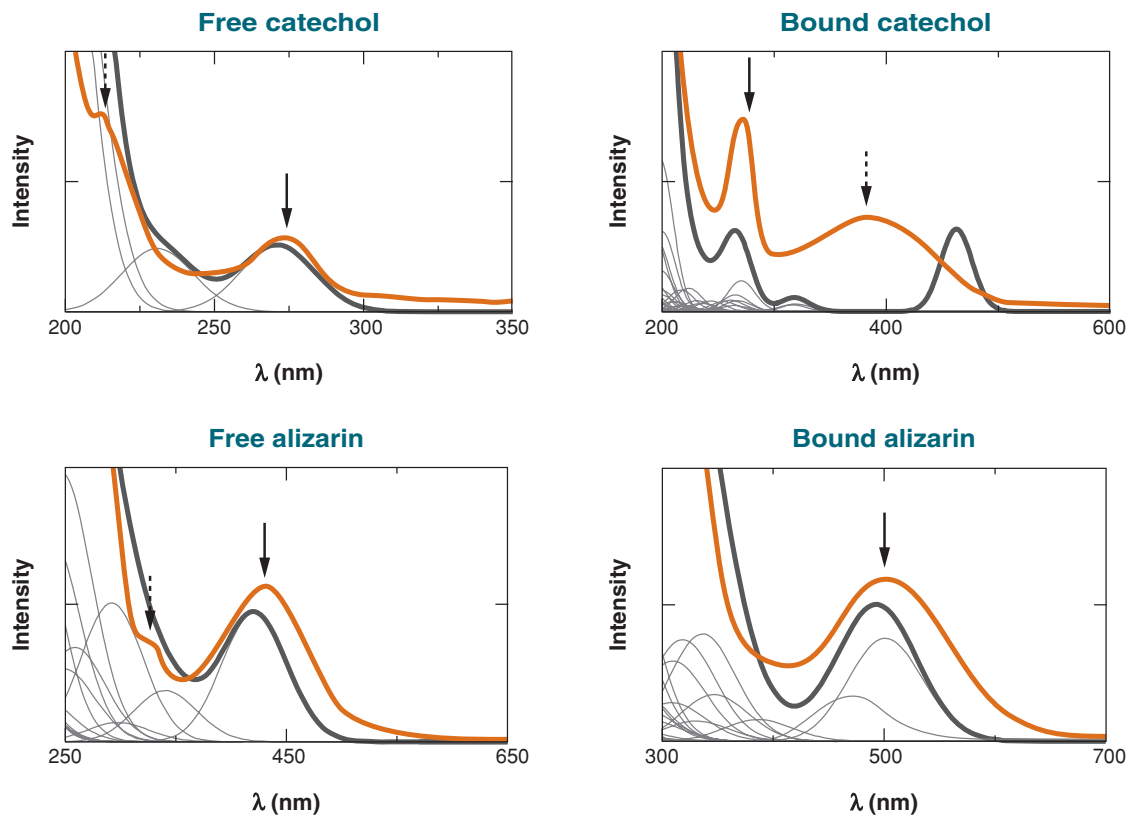


Figure 3

Experimental (*orange line*) and theoretical (*gray lines*) spectra of catechol and alizarin in free form (*left panels*) and bound to TiO_2 (*right panels*). Even though the catechol and alizarin molecules are closely related (see **Supplemental Figure 2**) and exhibit similar surface binding motifs, the binding has a dramatically different effect on their spectra. An entirely new band appears in the spectrum of the surface-bound catechol, in addition to the exactly repeated bands of the free catechol spectrum. In contrast, the alizarin spectrum red-shifts on binding, and no new bands arise. The origin of the spectral lines is revealed by the electronic-structure calculations (see also **Figure 4** and **Supplemental Figures 3** and **4**).

This defied the sequential ET mechanism that involved an excited state localized on the adsorbed chromophore. Intriguingly, despite the close relation of the alizarin molecule considered in the next section to catechol (**Supplemental Figure 2**), the electronic properties of these two molecules bound to TiO_2 are strikingly different.

3.2. Band Edge Photoexcitation of Alizarin on TiO_2

Alizarin and quinizarin are isomers that have similar electronic structures but bind to TiO_2 differently. Alizarin is closely related to catechol (**Supplemental Figure 2**) and, like catechol, prefers to bind to the semiconductor through two neighboring

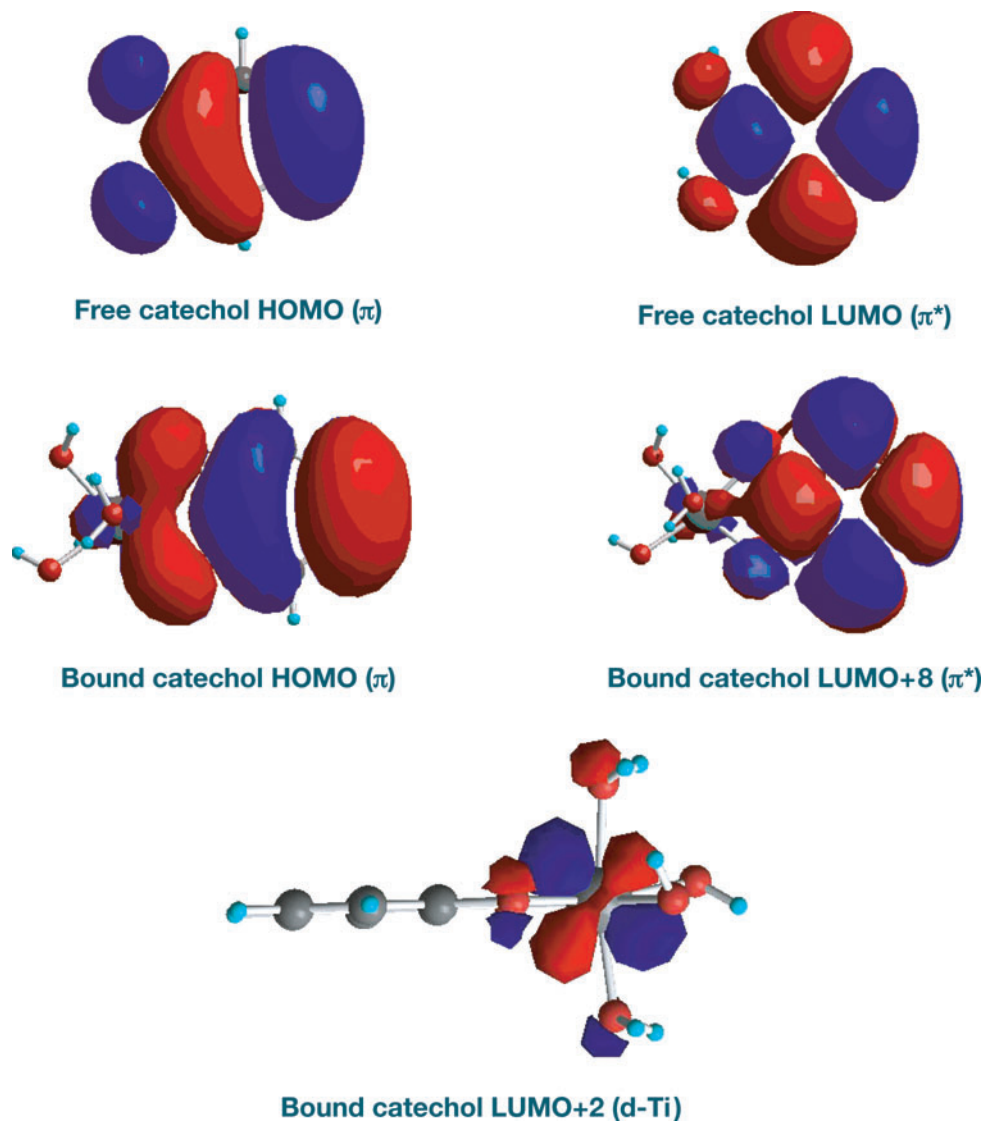


Figure 4

Images of the key orbitals of catechol in free state and bound to hydrated Ti^{4+} ion in solution. [The experimental spectrum of catechol bound to the hydrated Ti^{4+} ion and TiO_2 surface is similar (54, 74, 98).] The highest occupied molecular orbital (HOMO) of free catechol matches the HOMO of the bound system. However, the lowest unoccupied molecular orbital (LUMO) of free catechol matches the LUMO+8 of bound catechol. The LUMO of bound catechol and several orbitals above the LUMO are localized on titanium and are responsible for the new low-energy optical band (see **Figure 3**).

hydroxyl groups (**Figure 2**). Alizarin on TiO_2 was studied ab initio by Thoss and coworkers (98), as well as by our group (71–74). Quinizarin, an isomer of alizarin with the hydroxyl groups located on the opposite ends of the benzene ring, was investigated by Thoss and coworkers (98), as well as Makishima and coworkers (107).

Alizarin is a larger molecule than catechol, with a more extended π -electron system and, therefore, a smaller excitation energy. The presence of the electronegative quinone oxygens lowers the absolute values of the ground- and excited-state energies relative to an all-carbon molecule such as perylene, which is considered below. As a result, both alizarin and quinizarin have excited states close to the edge of the TiO_2 CB, giving rise to interesting features in electronic structure and dynamics. The optical activity for the charge-transfer excitations in the TiO_2 -bound alizarin is significantly smaller than in the catechol system, even though the chromophore-semiconductor coupling was exactly the same. The difference stems from the amount of mixing between the molecular excited π^* -orbital that provides the optical activity to the charge-transfer states and the Ti orbitals. The π^* -orbital of alizarin, spread over the entire molecule, was much more extended than the π^* -orbital of catechol, and, therefore, mixed less with the Ti orbitals (**Supplemental Figure 4**). In contrast to the case of catechol, a new optical band was not observed in the alizarin and quinizarin systems (58, 107). Instead, the transitions seen in free alizarin and quinizarin were red-shifted on binding to TiO_2 (**Figure 3**). This was a result of the lowering of the chromophore π^* -orbital energies caused by the mixing with the TiO_2 CB and a result of the presence of the weakly optically active charge-transfer transitions with alizarin bound to Ti through both hydroxyl groups (74, 98).

3.3. Perylene: A Large Organic Chromophore

Willig and coworkers (38–42, 44, 45) have extensively probed the perylene/rutile TiO_2 system, and they have also, in collaboration with May and colleagues (61–63), constructed a model Hamiltonian for the simulation of the electron-injection dynamics. Perylene is an all-carbon chromophore with an extended conjugated π -system. The experimental data indicate that the perylene photoexcited state is 0.5 eV above the bottom of the TiO_2 CB (44). This is in contrast to alizarin, which has smaller π -systems and larger photoexcitation energy gaps, but whose excited state is pulled down in energy by the electronegative quinone oxygens (**Supplemental Figure 2**) and is positioned near the bottom of the CB.

A detailed atomistic investigation of the binding and electronic structure of a combined perylene/ TiO_2 system requires large simulation cells and has not been carried out. The electronic structure of the isolated perylene chromophore has been studied by a number of authors, primarily using semiempirical approaches (108–110). Müllen and coworkers (108) investigated the nature of the excited states in oligorylene of varying sizes. Both the HOMO and LUMO of perylene are delocalized over the whole molecule and can be directly interpreted as linear combinations of the HOMO and LUMO of two naphthalene units (110). The LUMO that acts as the electron donor during the interfacial ET is polarized along the longer molecular axis of perylene and has three nodes perpendicular to the axis. The first excited state

of perylene is 2.8 eV above the ground state and is well isolated in energy from the next optically active excited state (108–109).

3.4. Benzoic Acid Has No States Within the TiO₂ Band Gap

Benzoic acid is a small π -conjugated chromophore similar in size to catechol. Lunell and coworkers (96) investigated the sensitization of anatase TiO₂ with benzoic acid and compared it with the catechol system considered in detail above. Quite surprisingly, and in sharp contrast to catechol and all other chromophores considered here, the spectra for TiO₂ remained unchanged after benzoic acid adsorption. Although the chromophore ground states typically fall within the TiO₂ energy gap, this was not the case with benzoic acid, whose ground state was approximately 1 eV below the VB edge. At the same time, the benzoic acid excited state was approximately 1 eV above the CB edge. Thus, benzoic acid did not insert any states within the band gap, and it did not create new optical bands that were lower in energy than the TiO₂ band gap absorption. Another difference between benzoic acid and other dyes is the strength of its coupling with the TiO₂ CB. The coupling through the benzoic acid carboxylic acid group is weaker than the coupling through the hydroxyl group seen with catechol and alizarin. The donor-acceptor-state mixing is, therefore, rather small. Photoexcited states distinctly localized on the chromophore can be clearly seen in the calculations, again in contrast to catechol, which has the same aromatic core as benzoic acid but whose excited states strongly mixed with TiO₂ CB states.

3.5. Bi-Isonicotinic Acid: The Transition Metal Ligand

Bi-isonicotinic acid is the most common ligand in the transition-metal chromophores (**Supplemental Figure 2**), which are considered in the next section. It is sufficiently small to be bound to bulk TiO₂ in a simulation cell and studied on a computer. Lunell and coworkers (102) investigated the electronic structure of bi-isonicotinic acid on rutile 110 using *ab initio* DFT. The ground state of bi-isonicotinic acid was located inside the TiO₂ band gap slightly above the VB. (Ligating bi-isonicotinic acid to a transition metal is expected to create a new higher-energy ground state closer to the middle of the gap.) The excited state of bi-isonicotinic acid, which is also the excited state of the chromophores composed of transition metals ligated with the acid, is rather deep inside the TiO₂ CB. This is supported by calculations that report a region of approximately 1 eV at the bottom of the CB, which was essentially free of adsorbate contributions (102).

3.6. Photochemically Robust Transition-Metal Chromophores

Chromophores comprised of a transition metal, most often Ru, and several ligands are the standard in photovoltaic applications. The metal can easily cycle between the oxidized and reduced states without significant photodamage to the chromophore, in contrast to the purely organic dyes, which become chemically active when oxidized. The ligands include at least one organic molecule with an extended π -electron system,

Semiempirical electronic-structure approaches: based on physical models and contain adjustable parameters determined by experimental data or ab initio approaches

Ab initio approaches: compute electronic properties starting from Columb's law, which is the most basic electronic interaction

such as isonicotinic acid (see above), and several smaller inorganic ligands (**Supplemental Figure 2**). The chromophore is attached to the semiconductor through the organic ligand. The smaller ligands participate in the regeneration of the neutral chromophore from the cation after the photoinduced ET. They assist in transferring the electron from a redox mediator in solution to the ground state of the dye. The HOMOs of the transition-metal-based chromophores are primarily composed of the *d*-orbitals of the metal, whereas the LUMOs are localized on the organic ligands. The photoexcitation induces the intrachromophore charge transfer, shifting the electron density toward the surface. The full system containing the metal, the ligands (which create an octahedral coordination around the metal), and a TiO₂ surface has not been detailed by an atomistic computational study. The isolated chromophores have been investigated rather comprehensively, however, both by semiempirical and ab initio approaches. These studies address several issues: (a) the origin of the bands in the chromophore optical absorption spectra that, ideally, cover a wide range of wavelengths; (b) the choice and optimization of the ligands in order to achieve both strong, broad absorption and efficient electron injection; (c) the solvent effects, including dye protonation and deprotonation by a change of pH; and (d) the triplet states.

***Cis*-bis(4,4'-dicarboxy-2,2'-bipyridine)bis(isothiocyanato)ruthenium(II).** *Cis*-bis(4,4'-dicarboxy-2,2'-bipyridine)bis(isothiocyanato)ruthenium(II) is a common dye and constitutes a good example of a transition-metal sensitizer chromophore. Siegbahn and coworkers (111) studied its electronic structure and spectrum using experimental methods and semiempirical INDO/S calculations. The calculated spectra matched the experimental spectra quite well. All the atomic orbitals of the organic ligands contributed somewhat to the three lowest energy absorption peaks, but the distribution was uneven: The lowest energy peak was dominated by the nitrogen *2p*-orbital contributions to the π -electron system, whereas the second peak was made up mostly of the ring carbon *2p*-orbitals. The atomic orbitals centered on the NCS⁻ ligands contributed to the highest energy valence orbital depopulated by the photon absorption. This orbital plays a key role in accepting an electron from the mediator in a Grätzel cell. Because the NCS⁻ ligands are directed away from the semiconductor and toward the solution, this type of dye should be particularly well suited to reduction from the electrolyte.

The black dye. Black dye is a trithiocyanato(4,4',4''-tricarboxy-2,2':6',2'-teripyridine)ruthenium(II) complex that can have different protonation states and numbers of counter ions. It is one of the most efficient light absorbers that can be used in Grätzel cells. The monoprotonated form gives the best results in experimental studies of black dyes adsorbed to TiO₂. The electronic-structure calculations of Aiga & Tada (112) showed strong absorption over the whole visible spectrum, as well as in the IR. The ligand-to-ligand charge-transfer states dominated in the low-energy part of the spectrum. These states corresponded to an electron on the teripyridine ligand and a hole on the NCS⁻ ligands. The higher-energy metal-to-ligand states also had an electron on the teripyridine ligand, but the hole was located on the metal center.

The authors argued that, because the dye attached to TiO_2 through the terpyridine ligand, the electron injection from both types of states should be fast. The calculated triplet excited states of black dye involved ligand-to-ligand charge transfer. The ET that can occur after an intersystem crossing to a triplet dye state should, therefore, be efficient as well.

Cis- versus trans-ruthenium complexes. Grätzel and coworkers (113) investigated the spectroscopic properties of a series of *cis*- and *trans*-Ru complexes and determined the theoretical spectrum of one set of complexes. The authors found that the three highest energy valence orbitals were made from predominantly Ru *d*-orbitals (65%–92% for the *trans* isomer and 70%–80% for the *cis* isomer), with moderate contributions from the organic ligand's π -orbitals. For the lowest unoccupied orbitals, the metal contributed only a small amount (1%–14% for the *trans* isomer and 3%–12% for the *cis* isomer). The vast majority was localized on the ligands, with 14%–32% of the low-lying π^* -orbitals on the carboxyl groups. In both the *cis* and the *trans* complexes, the intense band at approximately $16,900\text{ cm}^{-1}$ was a result of an excitation that had a strong contribution from a HOMO-LUMO transition. The *trans* complex also had a low-energy band at approximately $14,500\text{ cm}^{-1}$. The authors point out that the stronger absorption of light in the red and near IR regions for the *trans* complex could lead to Grätzel cells with better efficiency.

Variations in the ligands: 5,5'-dicarboxy- versus 4,4'-dicarboxy-2,2'-bipyridine; Cl^- , CN^- , and NCS^- . In an effort to move the spectral sensitivity of the efficient dye *cis*-Ru(4,4'-dicarboxy-2,2'-bipyridine) $_2(\text{NCS})_2$ toward the red, researchers changed the substitution on the bipyridine to produce *cis*-Ru(5,5'-dicarboxy-2,2'-bipyridine) $_2(\text{NCS})_2$. This second dye has a lower LUMO and a smaller energy HOMO-LUMO transition, thereby improving the response at longer wavelengths. This substitution, however, also produced a lower electron-injection efficiency in Grätzel cells at shorter wavelengths. To develop an understanding of what affected the dye energy levels, Mishra and coworkers (114) performed semiempirical calculations on two different classes of Ru-based complexes, *cis*-Ru(4dcb) $_2(\text{X})_2$ and *cis*-Ru(5dcb) $_2(\text{X})_2$, where $\text{X} = \text{Cl}^-$, CN^- , and NCS^- , and 4dcb and 5dcb stand for 4,4'-dicarboxy-2,2'-bipyridine and 5,5'-dicarboxy-2,2'-bipyridine, respectively. The calculations indicated that the 5dcb complexes had lower ground-state total energies than the corresponding 4dcb complexes and were therefore more stable. They also showed that the lowest-energy singlet excited state was substantially lower for the 5dcb dyes. The authors argued that ET events involving the first singlet excited state have a higher driving force for the 4dcb dyes than for the 5dcb dyes. A similar trend was observed for the lowest triplet state of the *cis*-Ru(5dcb) $_2\text{Cl}_2$ and the *cis*-Ru(4dcb) $_2\text{Cl}_2$ complexes, but the structures involving the other two inorganic ligands showed similar triplet-state energies. Going from 4dcb to 5dcb systems, the singlet-state energies decreased more than the triplet-state energies, and the singlet-to-triplet energy gap became smaller. The decrease of the singlet-triplet gap favors the intersystem crossing and therefore leads to more nonradiative decay, making the 5dcb dyes less-efficient photovoltaic converters.

Although the HOMOs were slightly lower in energy for the 4dcb structures than for the corresponding 5dcb structures, they had almost exactly the same shapes. In both cases the NCS^- substituted dye had less electron density on the Ru ion, with a large portion of the orbital localized on the S atoms. This structure makes it easier for a mediator in a Grätzel cell to deposit an electron onto the oxidized dye from the solution.

The authors analyzed the structure of the unoccupied orbitals of *cis*- $\text{Ru}(4\text{dcb})_2(\text{NCS})_2$ and *cis*- $\text{Ru}(5\text{dcb})_2(\text{NCS})_2$; the other chloro and cyano complexes exhibited similar trends. The LUMO and the LUMO+1 of the 4dbd structure were both involved in the first optical excitation and had enough electron density on the carboxylic groups to couple strongly to the CB of TiO_2 . The LUMO+2 and LUMO+3, both of which were involved in the second optical transition, had even more density on the carboxyl groups and should lead to better ET with higher frequency light. For *cis*- $\text{Ru}(5\text{dcb})_2(\text{NCS})_2$, the LUMO and the LUMO+1 were also involved in the first excitation and had substantial electron density on the carboxyl groups. The second excitation, however, involved LUMO+7 and LUMO+8 with less density on the carboxyl groups, resulting in a decreased chromophore-semiconductor coupling and a lower ET efficiency at shorter wavelengths for the 5dcb chromophores.

Effects of water and pH. *Cis*- $[\text{Ru}(4,4'\text{-COOH-2,2'}\text{-bipyridine})_2(\text{NCS})_2]$, also known as the N3 dye, exists in different forms at different pH. The spectral features are blue-shifted on moving from pH 1 to pH 9, whereby the fully protonated N3 dye becomes the fully deprotonated N3^{4-} . There is also a strong spectral dependence on the solvent. Selloni and coworkers (115) investigated the properties of both the N3 and the N3^{4-} complexes. The HOMO, HOMO-1, and HOMO-2 of the N3 dye arise from the antibonding combination of Ru t_{2g} , sulfur p -orbitals, and nitrogen lone pairs from the NCS^- ligands ($t_{2g} - \pi^*$). The three highest occupied orbitals for the N3^{4-} structure had the same character but were higher in energy. As with a number of the occupied energy levels, the N3^{4-} LUMOs are shifted upward in energy relative to the N3 orbitals. The deprotonation destabilized the orbitals localized on the bipyridine and COO^- components, which explains why the LUMOs with their larger localization on the deprotonated carboxylic groups were pushed up in energy, leading to a larger HOMO-LUMO gap (3.02 eV) for N3^{4-} versus that for the fully protonated form (2.31 eV).

Summary of the electronic-structure section. Photoexcitations encountered in the dye-sensitized TiO_2 systems can be classified into several types (see **Figure 1**). Most commonly, the chromophore ground state is located within the band gap of TiO_2 , and the photoexcited states are in resonance with the TiO_2 CB. With the exception of small chromophores connected directly to the semiconductor (such as catechol), the photoexcited states are well localized on the semiconductor and do not mix appreciably with the CB and surface states. The injection dynamics proceeds in two distinct steps, including photoexcitation followed by ET. In systems such as catechol/ TiO_2 with exceptionally strong chromophore-semiconductor coupling, the photoexcitation already induces ET into a surface state. The photoexcited states of

some chromophores, such as alizarin and quinizarin, are located close to the bottom of the TiO₂ CB. These cases present the most complicated injection dynamics because they involve both localized and mixed states. Transition-metal-based chromophores possess a more complex electronic structure than the purely organic chromophores. The photoexcitation typically, but not necessarily, involves intrachromophore charge transfer. The metal creates strong spin-orbit coupling, promoting intersystem crossing into triplet states. Apart from the lower energy of the triplet excited states than the singlets, similar ET mechanisms can be expected from states of either spin.

4. QUANTUM MODELS OF ELECTRON-VIBRATIONAL DYNAMICS

A quantum-mechanical description of the electronic and vibrational dynamics involved in the ET can be achieved using simplified models of the interface (40, 42, 61–65), which are constructed and tested against experimental data and electronic-structure calculations. The dynamics that follows from such models can be treated at the full quantum level. The model parameters have clear physical meaning and can be varied to probe and characterize various injection regimes.

4.1. Theoretical Aspects of Model Hamiltonians

Model Hamiltonians used to describe the interfacial ET dynamics comprise several parts that have well-defined physical origins and have been tested with many other systems. Although the details vary from author to author, the general structure, known in the interfacial ET community as the Anderson-Newns Hamiltonian, is as follows (62, 64): The full Hamiltonian, H , is split into the electronic, H_{el} , and nuclear, H_{nucl} , contributions, and, sometimes, a time-dependent term describing the interaction with the laser pulse, $H_{laser}(t)$:

$$H = H_{el} + H_{nucl} + H_{laser}(t). \quad (1)$$

The electronic part includes the energies, ε_a , of the ground, g , and excited, e , chromophore states, the energies of the quasi-continuum of TiO₂ CB states, $\{k\}$, and the coupling between the chromophore excited state and CB, V_{ke} :

$$H_{el} = \sum_{a=g,e,\{k\}} |\phi_a\rangle \varepsilon_a \langle \phi_a| + |\phi_k\rangle V_{ke} \langle \phi_e| - |\phi_e\rangle V_{ek} \langle \phi_k|. \quad (2)$$

The nuclear Hamiltonian describes molecular and semiconductor vibrational modes in the harmonic approximation, and includes the electron-vibrational coupling, c_l :

$$H_{nucl} = \frac{1}{2} \sum_l [p_l^2 + \omega_l^2 x_l^2 + |\phi_e\rangle 4c_l x_l \langle \phi_e|], \quad (3)$$

where p_l , x_l , and ω_l are the momentum, position, and frequency of mode l , respectively. The frequency distribution of the vibrational modes, as well as the electron-vibrational coupling, is specified by the spectral density

$$\mathcal{J}(\omega) = \frac{\pi}{2} \sum_l \frac{c_l^2}{\omega_l} \delta(\omega - \omega_l), \quad (4)$$

Marcus theory: the generally accepted theory of electron transfer developed in parallel by Levich and Dogonadze and extended further by Jortner, Gerischer, and many others

which can be given a simple analytical form or computed explicitly from an atomistic, classical-mechanical calculation. The reorganization energy λ that enters the Marcus theory of ET is related to the spectral density via

$$\lambda = 2 \sum_l \frac{c_l^2}{\omega_l^2} \quad (5)$$

$$= \frac{4}{\pi} \int d\omega \frac{\mathcal{J}(\omega)}{\omega}. \quad (6)$$

A few vibrational modes can be treated explicitly, whereas the rest of the vibrations are regarded as a bath and are integrated out. The model includes two kinds of coupling: the chromophore-semiconductor electronic coupling, V_{ek} , and the electron-vibrational coupling, c_l . In the adiabatic representation, the off-diagonal elements, V_{ek} , of the electronic Hamiltonian (Equation 2) are eliminated by the diagonalization of H_{el} . Setting $c_l = 0$ creates a purely electronic model of the transfer.

4.2. Applications of Model Quantum Dynamics

Using a model Hamiltonian of this kind and a density-matrix formalism, Ramakrishna & Willig (40) obtained an expression for the pump-probe signal in a chromophore-semiconductor system. They modeled the decay of the excited state into a continuum of semiconductor states for various relative energy positions and bandwidths, with the assumption that the ET was much slower than the pulse durations. They also assumed the reorganization energy of the ET process was negligible, which meant the lifetime of the excited state was dependent only on the density of acceptor states at the energy of the donor, not on the dynamics created by the two laser pulses. In most cases, the decay was fit by exponential functions. Ramakrishna & Willig (40) did obtain oscillations in the pump-probe signal owing to vibrational coherences detected in their experimental work.

May and coworkers (42, 61–63) analyzed the ET dynamics in a chromophore-semiconductor system using a model Hamiltonian and a time-dependent Schrödinger approach. Extending the work of Ramakrishna & Willig (40), they addressed the effect of the reorganization energy, along with the energy of the donor level, on the vibronic coherence produced in the initially excited chromophore.

Increasing the reorganization energy associated with the molecular cation formation increased the contribution of the Frank-Condon factors to the population decay. This slowed the ET and caused oscillations that were a result of the movement of the wave packet toward and away from the donor-acceptor crossing point. Changing the position of the injecting level, May and coworkers found two types of behavior. In the wide band limit, when the injecting level was in the middle of the band, a sufficiently large range of allowed vibrational levels provided a fast and unrestricted exchange of vibrational energy between the ionized molecule and the injected electron. In cases in which the injecting level was close to the band edge, a limited vibrational range resulted in slower decays with pronounced oscillations.

The authors also investigated the effect of varying the initial vibrational wave packet, which can be achieved in experiments by changing the nature of the laser

pulse. Only certain vibronic levels were significantly populated after the excitation. In the wide band limit, each of them decayed with the same rate. Different distributions, therefore, led to similar ET dynamics. Close to the band edge, however, the dynamics were dependent on the initial distributions. Distributions with large populations of the lower vibronic levels close to the bottom of the CB led to slower, step-wise decay. The DOS and the electronic coupling influenced the ET dynamics as well. When the DOS and the coupling change slowly over the relevant energy range, ET is well described by the pure electronic limit without vibrational contributions. When the DOS and the coupling vary significantly, however, the decay into the semiconductor states also depends substantially on the vibrational Frank-Condon factors. The atomistic simulations described below show that the chromophore-semiconductor coupling varies much more with energy than the TiO_2 DOS. The conclusions of the quantum models and atomistic quantum-classical studies together indicate that vibrational dynamics should have a profound effect on the ET.

Wang and coworkers (64, 65) studied the ET rate between the dye and the semiconductor using an Anderson-Newns-type model with a tight-binding parameterization. They analyzed the quantum-dynamical effects with a self-consistent hybrid method. To study the influence of the vibrational motions in their system, the authors used two different models: (a) a normal-mode model in which all the vibrational degrees of freedom were coupled to the electronic degrees of freedom in the same way and (b) a reaction-coordinate model, which focused on certain reaction coordinates and treated the others as a bath (64).

In the normal-mode model, including the coupling to vibrational modes led to slower, incomplete decay dynamics. Some of the energy of the excited electron was transferred to vibrational modes, and was, therefore, not available for the injection into the semiconductor. Investigating the effect of the chromophore-semiconductor coupling strength on the electron injection in the normal-mode model, the authors found, as one would expect, that increasing the coupling led to faster injection with a larger yield for moderate coupling. A very strong coupling, however, created a bound state below the CB, leading to incomplete transfer. The bound state appeared even for moderate electron-semiconductor coupling if the original chromophore state was close to the CB edge. The effect of the bound state was most pronounced in the absence of an electron-vibrational interaction. They observed the same general trend in the presence of the interaction, but the influence of the vibrational motions often led to significantly different dynamics.

The reaction-coordinate model allowed the authors to determine the influence of coherent vibrational motions on the electron injection. They found that including the vibrational coupling in this model led to slower decay, with steps that had the frequency of the reaction coordinate. This was a result of the coherent motion of the vibrational wave packet into and out of regions with crossings between donor and acceptor states. Increasing the coupling to the bath led to faster vibration relaxation inside the chromophore and therefore slower, less complete decay, particularly if the photoexcited state was close to the band edge. Very strong couplings to the bath caused damped coherent vibrational motion and produced no steps in the decay. The authors found an interesting correlation between the equilibrium geometries of the

chromophore ground–electronic state and the amount of vibrational coherence in the ET signal. If donor ground states had the same equilibrium geometry as the acceptor states, then the donor ground and excited states were significantly displaced, leading to large vibrations in the excited state. The relationship between the energy of the photoexcited state and the injection yield found by Wang and coworkers (64, 65) agrees with the conclusions of May and coworkers (42, 61–63). In both simulations, donor states close to the band edge led to less complete transfer. Both groups found that the ET is particularly sensitive to the magnitude and energy dependence of the chromophore–semiconductor coupling, as well as to the vibrational dynamics. It is possible to determine the effect of the coupling strength and the vibrational dynamics directly using atomistic simulations.

5. AB INITIO STRUCTURE COMBINED WITH SEMIEMPIRICAL DYNAMICS

Atomistic studies of the electron-injection dynamics are based on fundamental models of electron–nuclear interaction developed either *ab initio* or semiempirically. Starting from the fundamental Coulomb interaction, *ab initio* treatments solve the many-body electronic problem in the presence of an external classical potential owing to nuclei. Because an exact solution of the many-body Schrödinger equation can be achieved with only a few electrons, approximations become necessary, the most practical of which are based on DFT, which extends beyond the mean-field description and includes electron correlation. In contrast to wave-function-based approaches that include nonlocal electron exchange, DFT constructs local or nearly local functionals of electron density that can be implemented easily with infinite systems that use periodic boundary conditions and plane-wave basis sets. Semiempirical schemes use the same types of approximations for the many-body problem as *ab initio* approaches, but instead of computing the Hamiltonian matrix explicitly by using a basis set, semiempirical calculations treat Hamiltonian matrix elements as parameters determined by experimental data and *ab initio* calculations.

Batista and coworkers (66, 67) investigated the dynamics of electron injection from the higher excited states of catechol to TiO_2 , using a combination of *ab initio* and semiempirical approaches. The catechol- TiO_2 system is suitable for theoretical studies for a number of reasons: It is small; its lowest energy excitation promotes the electron directly into the semiconductor (see Section 3.1); and its higher energy excitations provide good examples of the more typical photoexcitation–followed-by-injection scheme. Modeling the catechol system can lead to a better understanding of larger systems that include substituted catechol chromophores and have high-incident photon-to-current conversion efficiencies.

Batista and coworkers used *ab initio* DFT molecular dynamics to obtain nuclear configurations for semiempirical ET calculations. The simulation cell consisted of catechol attached to the anatase 101 TiO_2 surface through a dissociative adsorption between both hydroxy groups and two neighboring pentacoordinated Ti^{4+} ions. The semiconductor layer had 32 TiO_2 units with the top and bottom surfaces terminated by hydrogen atoms. Periodic boundary conditions led to a surface coverage of

$1 \mu\text{mol m}^{-2}$. The DFT simulations provided the opportunity to analyze the timescales of the vibrations to see if they would influence the ET. The authors concluded that the high-energy oscillations were a result of surface O-H stretches and catechol C-H stretches that would not affect the ET. They also argued that the low-energy oscillations were too slow, approximately 40 fs, to interfere with the sub-10-fs transfer they eventually calculated for the system.

The authors used a semiempirical extended Hückel approach to propagate the excited wave function. The DOS calculated from the diagonalization of the extended Hückel Hamiltonian showed there were states located energetically in the CB that had strong catechol character. By placing the electron in one of these catechol states and propagating the system in time, the authors were able to determine both the timescale of ET and the spatial evolution of the charge density. By extending the DFT simulation cell in different crystallographic directions, the authors obtained larger cells for the semiempirical studies and tested the anisotropy in the ET process. For systems in which the excited electron was placed in the catechol LUMO, the cells that had been extended in the [010] and the [101] directions produced ET that was fit by a 6-fs exponential. The cell extended in the $[-101]$ direction, however, produced ET that had two exponential time constants: a 6-fs initial decay followed by a 38-fs decay. This indicated there were two steps to ET, with the second step involving an anisotropic delocalization. Projections of the time-dependent charge distribution showed that the first step was a localization of the excited electron on the Ti^{4+} ions attached to the catechol, and even more on the neighboring hexacoordinated Ti^{4+} ion. The excited electron density then diffused along the [101] direction, away from the surface, before spreading in the [010] direction. The spread in the $[-101]$ direction was much slower, explaining the slower time constant for the $[-101]$ extended system.

ET from the catechol LUMO+1 state was markedly different. In this case the initial charge localization on the TiO_2 surface occurred on the Ti^{4+} ions attached to the catechol, with almost no density on the neighboring hexacoordinated Ti^{4+} . The subsequent delocalization within the semiconductor slab was also proceeded by a different mechanism: The charge quickly spread along the surface of the TiO_2 , in the [010] direction, before moving deeper into the slab in the [101] direction. The ET was fit by a 3-fs exponential time constant for cells extended in any of the three directions, with no slower time component present, even for the $[-101]$ case.

6. AB INITIO NONADIABATIC MOLECULAR DYNAMICS

Nonadiabatic molecular dynamics (NAMD) provides a direct strategy for modeling coupled electron-vibrational dynamics in real time and at the atomistic level (116–124). The electronic degrees of freedom are described quantum-mechanically by many-body electronic-structure theory, whereas vibrations are considered using classical mechanics or semiclassically as justified by the separation of electronic and nuclear masses and timescales. The atomistic descriptions reproduce the actual interface as closely as possible, by taking explicit account of the chemical structure of chromophores, chromophore-semiconductor binding, surface conditions, conformational and chemical changes, and disorder.

Extended Hückel: the simplest electronic structure approach named after E. Hückel that contains a minimal number of parameters directly related to experimental data

Nonadiabatic molecular dynamics (NAMD): an advanced form of molecular dynamics, in which atomic motions can induce transitions between electronic states

Time-dependent density-functional theory:

an extension of time-independent density-functional theory that evaluates electronic response to time-dependent perturbations such as atomic motions and light

KS: Kohn-Sham

6.1. Theoretical Aspects of Nonadiabatic Molecular Dynamics

Our group (68–75) studied the ET in Grätzel cells with ab initio NAMD. We performed electronic-structure and molecular dynamics simulations of chromophore/TiO₂ systems with DFT in the plane-wave basis using the VASP code (125–127). The NAMD functionality was added to the standard code distribution, creating a time-dependent DFT (128) version of the code. Within the Kohn-Sham (KS) formulation, the charge density $\rho(\mathbf{r}, t)$ was described by a sum over the KS orbitals $\psi_n(\mathbf{r}, t)$ occupied by N_e electrons:

$$\rho(\mathbf{r}, t) = \sum_{n=1}^{N_e} |\psi_n(\mathbf{r}, t)|^2. \quad (7)$$

The evolution of the density caused by the moving ions led to the coupled equations of motion for the KS orbitals,

$$i \hbar \frac{\partial}{\partial t} \psi_n(\mathbf{r}, t) = H(\mathbf{r}, \mathbf{R}, t) \psi_n(\mathbf{r}, t), \quad n = 1, 2, \dots, N_e. \quad (8)$$

We then expressed the single electron orbitals on the basis of adiabatic KS orbitals $\phi_k(\mathbf{r}, \mathbf{R}(t))$ that were obtained from a time-independent DFT calculation at the appropriate point along the classical trajectory of the atoms $\mathbf{R}(t)$. For the photoexcited (PE) electron,

$$\psi_{PE}(\mathbf{r}, t) = \sum_k c_k(t) \phi_k(\mathbf{r}, \mathbf{R}(t)). \quad (9)$$

Substituting this into Equation 8 led to the equation for the coefficients,

$$i \hbar \frac{\partial}{\partial t} c_j(t) = \sum_k c_k(t) (\varepsilon_k \delta_{jk} + d_{jk}), \quad (10)$$

where ε_k is the energy of the adiabatic orbital k , and d_{jk} is the NA coupling between orbitals j and k (129). Equation 10 was propagated using the second-order differencing scheme (130). Further details can be found in References 68, 69, and 75.

We carried out the simulations with several chromophores dissociatively adsorbed to a slab of rutile TiO₂, whose surfaces were terminated by hydrogen and hydroxyl groups (**Supplemental Figure 5**). We determined the extent of ET by the fraction of the photoexcited electron that left the dye, which was computed by integrating the electron density of the photoexcited state over the region of the simulation cell occupied by the dye. We then defined the adiabatic and NA contributions to ET by separating the change in the one-electron density into the change in the localization (adiabatic ET) and the changes in the occupations (NA ET) of the adiabatic states (68). The separation between the adiabatic and NA ET mechanisms addressed the question raised by the experimental groups (34, 38, 39, 47–50) on whether the observed fast injection was mediated by a strong chromophore-semiconductor coupling (adiabatic ET) or a large density of TiO₂ acceptor states (NA ET).

We fit the time-dependent ET coordinate with the exponential

$$\text{ET}(t) = \text{ET}_f (1 - \exp[-(t + t_0)/\tau]), \quad (11)$$

where ET_f is the final amount of ET. The fit took into account that photoexcitation had already caused a partial ET to occur, $\text{ET}_{t=0} = 1 - \exp(-t_0/\tau)$. The constant

t_0 represents the amount of time the system had advanced along the ET reaction coordinate because of the photoexcitation.

6.2. Electron Injection from Isonicotinic Acid at Low Temperature

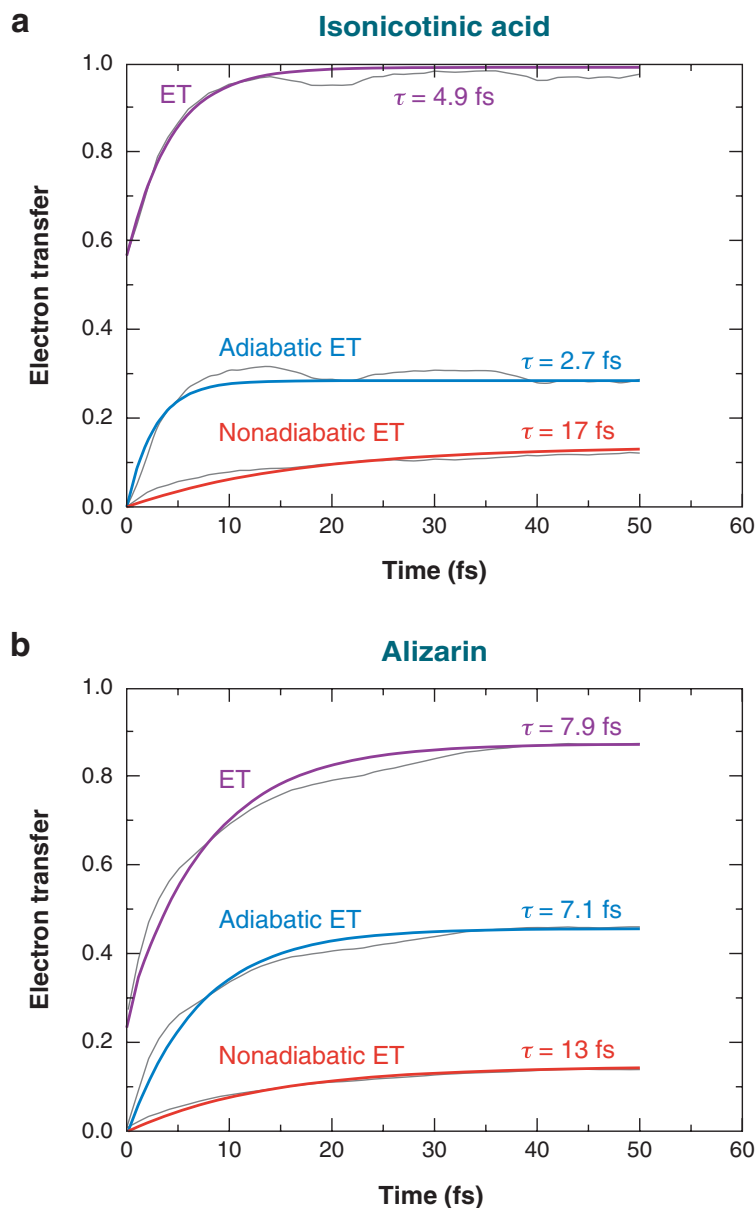
The first set of simulations investigated electron injection from isonicotinic acid at 50 K (68), which represents a typical ligand in a transition-metal chromophore under cold, ultrahigh vacuum conditions. In this system, the photoexcited state was well within the CB of the TiO₂. Despite a large DOS at the excited-state energy, only a small number of TiO₂ states were capable of interacting with the chromophore and accepting the electron. In addition to being at the correct energy, the acceptor states also had to be localized on the surface near the dye-adsorption point. These states were within the first three titanium layers, with approximately 20% of the density on a single Ti surface atom. The adiabatic and NA ET mechanisms functioned during different periods of the simulations. NA ET relied on a weaker coupling of the dye state to a number of semiconductor states and could occur both near an avoided crossing and in extended regions of NA coupling away from a crossing. Adiabatic ET took place at avoided crossings where there was strong coupling between the dye state and a single semiconductor state. Both mechanisms contributed significantly to the ultrafast ET. Averages of many runs gave general trends. In the isonicotinic acid–TiO₂ system at low temperature, the NA pathway dominated, particularly at early times, and was fit by an exponential with a 20-fs time constant. In the beginning, only a small fraction of the transfer occurred by way of the adiabatic mechanism. The adiabatic exponential time constant was 40 fs. The fraction of adiabatic transfer, however, increased during the course of the simulation, to the point where at 50 fs it was almost as important as the NA ET (68).

6.3. Electron Injection from Isonicotinic Acid at Ambient Temperature

We also explored the ET dynamics of the isonicotinic acid chromophore at ambient temperatures (69, 70). At the elevated temperature, the energy of the dye state oscillated by several tenths of an electron volt as a function of time (**Supplemental Figure 6**). This was small relative to the initial excitation, but it made a substantial difference in the dye-state position relative to the CB. The CB DOS increased with energy in this region, so an increase in the dye energy tended to lead to a larger number of states with which the dye could interact. The well-pronounced oscillation of the photoexcited-state energy was induced by the C–C stretching modes and resulted in a bimodal distribution of the photoexcited-state energy at the initial time (69). There were no corresponding high- and low-energy regions in the low-temperature simulations (68). At ambient temperature, the adiabatic ET was both faster (2.7 fs) and had a larger contribution to the overall ET than the NA ET (17 fs). There was also a much larger contribution from the photoexcitation itself, with over 50% of ET happening during the photoexcitation (**Figure 5**).

Figure 5

The electron-transfer (ET) dynamics averaged over ensembles of initial conditions for (a) isonicotinic acid and (b) alizarin systems at room temperature. The ET coordinate is defined by the fraction of the electron that has left the dye. The injection starts from the photoexcited states that are already significantly delocalized onto the semiconductor. The degree of delocalization is larger with isonicotinic acid because its excited state is higher in energy and interacts with more states in the TiO_2 conduction band. The adiabatic injection mechanism dominates in both cases owing to strong chromophore-semiconductor coupling. The nonadiabatic mechanism is more important in the isonicotinic acid system, where the coupling through the $-\text{COOH}$ group is weaker than the coupling through the two $-\text{OH}$ groups in alizarin.



6.4. Alizarin- TiO_2 Electron Transfer

In our later work, we explored the ET dynamics of alizarin attached to TiO_2 at ambient temperature (70–75). This system is particularly interesting because the ET is ultrafast, 6 fs measured experimentally (59), but the dye excited state is at the edge of the CB, where the TiO_2 DOS is lowest (Figure 6).

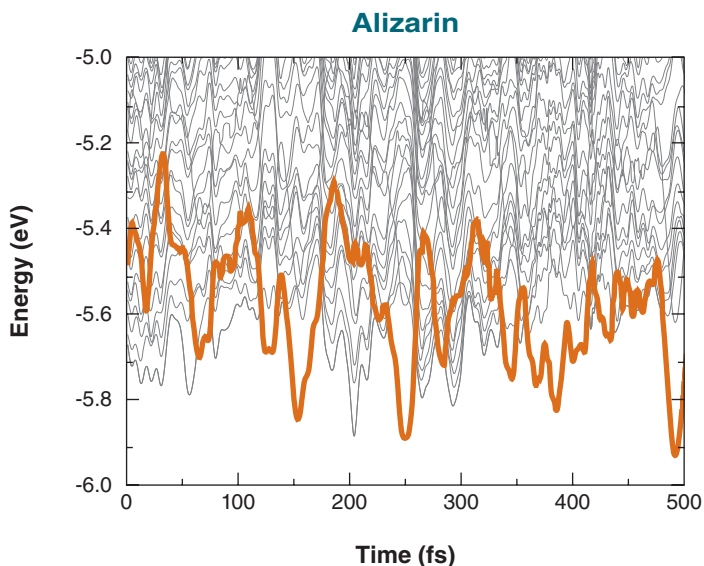


Figure 6

Vibrationally induced dynamics of the photoexcited-electronic state in the alizarin system. The orange line shows the photoexcited-state energy, and the gray lines show energies of conduction band (CB) states. The alizarin state frequently crosses the CB edge, oscillating over a range of frequencies.

Variation in initial conditions and dye-semiconductor coupling owing to phonon motions.

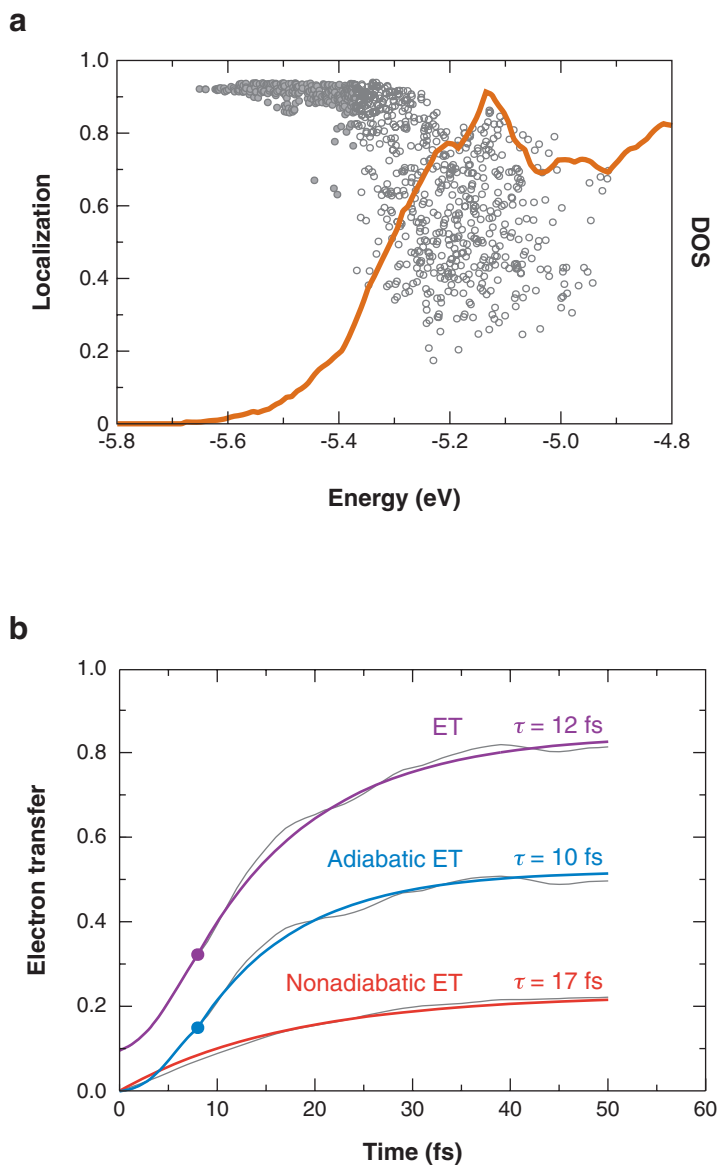
As with the isonicotinic acid system at the ambient temperature, the photoexcited-state energy of alizarin oscillated by a fraction of an electron volt. This created two types of initial conditions: (a) high-energy initial conditions in which the state was above the CB edge and (b) low-energy initial conditions in which the state was below the band. Photoexcited states below the band coupled much less to the semiconductor states and tended to be localized almost entirely on the chromophore. As the state moved into the band and the DOS increased, the degree of coupling and mixing between the chromophore and TiO₂ states tended to increase as well (Figure 7). An analysis of the frequencies of oscillations of the dye state energy and localization showed that changes in the energy (Figure 6) were a result of atomic motions in the chromophore. However, changes in the localization (Supplemental Figure 7), which depended on the strength of the chromophore-semiconductor coupling, were a result of both chromophore and surface hydroxyl motions (compare the frequencies present in Supplemental Figures 6b and 7b). This showed that the electronic coupling between alizarin and the semiconductor varied greatly even within a small energy range. The substantial variation in the chromophore-semiconductor coupling was further supported by the large spread of localization of the photoexcited state on alizarin presented in Figure 7a.

The electron-transfer mechanism. The ET dynamics of the alizarin system, averaged over all initial conditions (Figure 5b), were similar to the ambient-temperature isonicotinic acid results averaged over all initial conditions (Figure 5a): The total ET occurred on a sub-10-fs timescale; there was a substantial amount of charge transfer during photoexcitation (25%); the adiabatic mechanism had a faster rate (7.1 fs) than the NA mechanism (13 fs); and the adiabatic ET was a much larger fraction of the

Figure 7

(a) Distribution of photoexcited-state energies (circles) in the alizarin system relative to the TiO_2 density of states (DOS) (orange line). As the DOS increases with energy, the localization of the photoexcited state on alizarin decreases.

(b) Electron-transfer (ET) dynamics averaged over the initial conditions below the conduction band (CB) edge (filled circles in a). The initial nonexponential rise of adiabatic ET describes the time required for a photoexcited state below the CB to enter the band (see Figure 6).



total transfer. Further ET features were revealed by separately averaging over the high- and low-energy initial conditions corresponding to the photoexcited states inside and below the TiO_2 CB. Averaged over just the higher-energy initial states (Supplemental Figure 7), both the total and adiabatic ET were faster, 3.6 and 3.2 fs, respectively; the adiabatic mechanism was more dominant relative to the NA ET; and there was a larger amount of initial charge transfer. The overall shape of the ET curves for the higher-energy initial conditions was similar to the average data

(Figure 5*b*). The low-energy photoexcited states were substantially different (Figure 7), however. The total ET and the adiabatic ET were not exponential for the first 8 fs, and they were best fit by an inverted Gaussian. This was a result of the fact that the initial state could not encounter an avoided crossing and therefore could not transfer adiabatically until ion motions drove it into the CB. After this initial waiting period, the transfer could be fit by an exponential, 10 fs for the adiabatic ET and 12 fs for the total ET. The NA mechanism, which could occur in regions with no avoided crossings, was fit with an exponential for the entire run. The lower DOS at these low energies corresponded to fewer states to couple to, so the NA ET was substantially slower, 17 fs. Even with this slower rate, the NA component was relatively large because of the initial delay in the adiabatic transfer and its slower rate once the photoexcited state entered the CB. Because the initial states at energies below the CB were well localized on the chromophore fragment, the degree of initial charge transfer was small, under 10%.

Examples of electron-injection events. The substantial variation in individual ET events seen with all systems is illustrated in Figure 8 for the alizarin-TiO₂ interface. In the most typical example for both alizarin and isonicotinic acid (Figure 8), the photoexcited state is located within the TiO₂ CB, and the injection occurs ultrafast and primarily through the adiabatic mechanism. Over time, the injected electron delocalizes from the original surface-acceptor state into the bulk by NA hopping between the states, thereby increasing the contribution of the NA mechanism. In the second example (Figure 8), the initial injection is also fast and occurs adiabatically. The difference between the two examples arises from the fact that the photoexcited state is close to the edge of the CB and is able to leave the band before the injected electron has had a chance to delocalize into the bulk by the NA mechanism. Adiabatic crossing of the same transition state, which has led to the electron injection, now results in the transfer of the electron back onto the chromophore. This pattern of adiabatic injection followed by adiabatic back-transfer occurs several times over the course of the simulation and is superimposed on a much slower NA ET that is practically irreversible. The third example (Figure 8) is typical only of alizarin. Here the photoexcited state is well below the TiO₂ CB edge, and essentially nothing happens with the electron until the photoexcited state crosses into the band. Only a small and slow NA-injection component is seen during the first 20 fs of the simulation. Crossing the CB edge results in a rapid adiabatic transfer. Photoexcitation below the CB remarkably can lead to fast and efficient electron injection (71, 72).

Electron evolution after the injection. Following the photoexcitation and the chromophore-semiconductor ET, the electron delocalizes into the semiconductor bulk and, eventually, finds its way back to the chromophore ground state. The electron injection occurs between the dye and a TiO₂ state primarily restricted to the first three surface layers in the alizarin system (71, 72). With isonicotinic acid (68, 69), a single Ti atom can constitute 20% of the acceptor surface state. Preliminary results indicate the spreading of the electron population from the surface into the

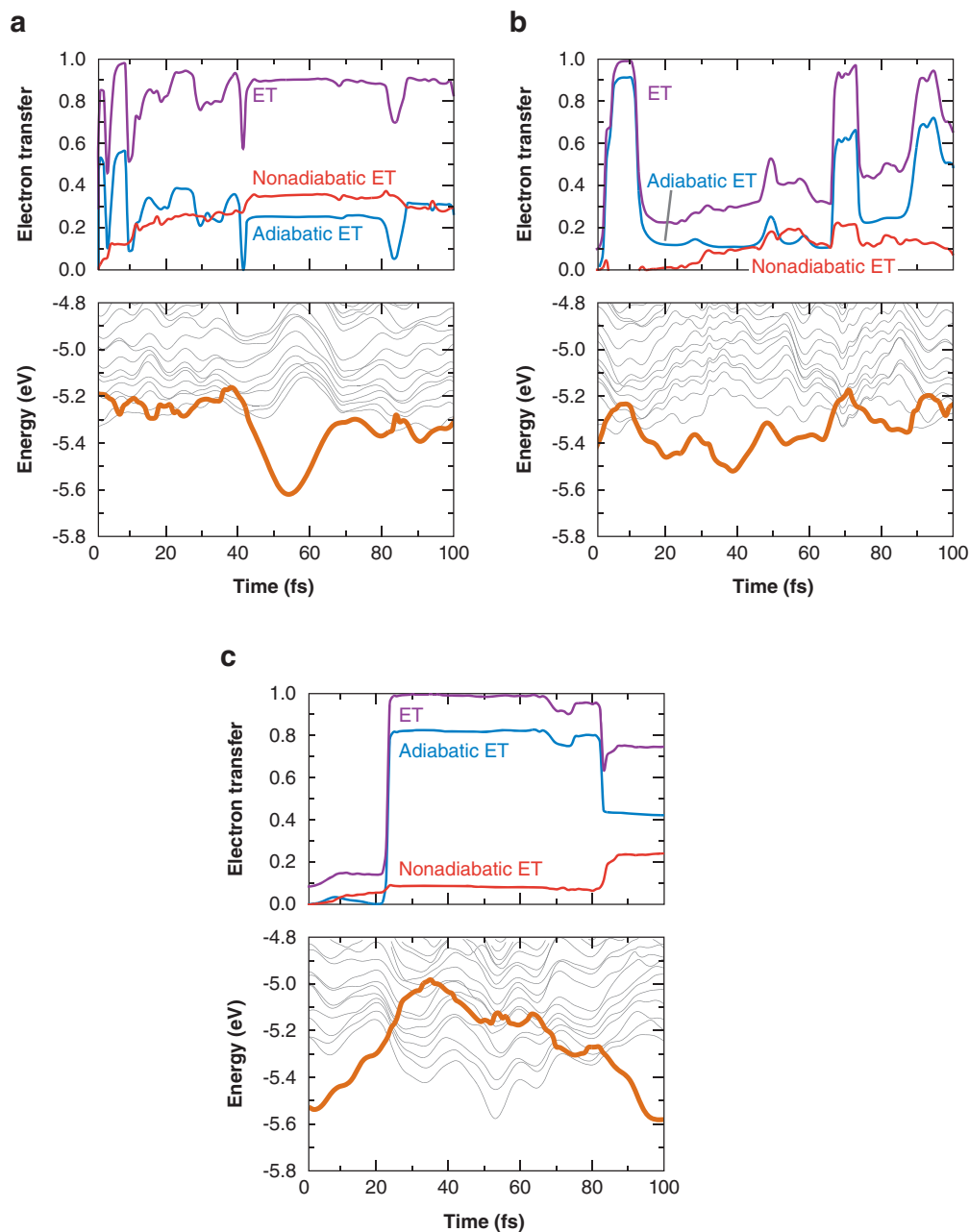


Figure 8

Examples of individual electron-transfer (ET) events in the alizarin system. The bottom panels show the evolution of the photoexcited-state energies, as in **Figure 6**. The top panels present the ET progress, as in **Figure 5**. The large variation in the individual ET events seen in these examples is typical with all chromophore-semiconductor systems.

bulk occurs on a 100-fs or longer timescale, which is in agreement with the available experimental data (43, 131).

Owing to the high-surface area of dye-sensitized TiO₂, an electron delocalized inside bulk TiO₂ has a high probability of finding a surface. Trapping at the surface can result in ET back onto the chromophore or the electrolyte mediator, which normally brings the electron from the counter-electrode to the dye. Assuming the electron is trapped inside the first five surface layers (as represented by the simulation cells in **Supplemental Figure 5**), the surface-hopping simulation shows that the back-transfer to the ground state of alizarin occurs two orders of magnitude slower than the injection (75). The result is in agreement with the experimental data on the alizarin-ZrO₂ system (58), in which the electron remains trapped at the surface because the semiconductor CB is significantly higher in energy than the alizarin photoexcited state. The back-transfer is preceded by a 100-fs relaxation to the bottom of the TiO₂ CB. The back-transfer of the trapped electron is much faster than the time needed by the electron to travel through nanoporous TiO₂ to the primary electrode.

6.5. Complete Sequence of Electron-Transfer Events

The real-time *ab initio* simulations indicate that the ultrafast photoinduced electron injection from a chromophore to TiO₂ is followed by a rapid delocalization of the electron into the bulk that competes with electron relaxation to the bottom of the TiO₂ CB. Both delocalization and relaxation occur on a 100-fs timescale. If the electron is trapped at the surface (either immediately after the injection or following some evolution in the bulk), it returns to the dye ground state on a picosecond timescale.

7. CONCLUSIONS AND OUTLOOK

The chromophore-TiO₂ interface is an excellent case study for elucidating the issues that arise when localized molecular species are combined with extended bulk materials. Such configurations have become increasingly common in recent years, as molecular and solid-state domains have converged, with molecules assembled into ever more complicated mesoscopic structures, and periodic systems miniaturized on the nanoscale. Understanding the molecule-crystal interfaces is one of the most challenging problems in many fields and applications, including photovoltaics, photo- and electrochemistry, molecular electronics, photography, detection tools, bioanalytical chemistry, and biomechanics. Molecules and bulk materials are opposites in nearly every respect: The former have discrete electronic states, whereas the latter form energy bands; the fraction of high-frequency vibrational modes is much higher in molecules than in inorganic semiconductors such as TiO₂; and the electron-phonon coupling and excitonic effects are much stronger in finite systems. The problem in describing the interface is complicated further by the drastic differences between chemists' and physicists' models for treating molecules and bulk materials, respectively.

Analysis of the available theoretical results on the structure, electronic properties, and electron-vibrational dynamics in the chromophore-TiO₂ systems indicates

that the chromophore creates a local perturbation within the extended TiO_2 system. Most of the experimental data characterizing the effect that bulk TiO_2 has on chromophores can be modeled and understood with relatively small-scale calculations that include moderate-sized portions of the semiconductor. A cluster representation of the semiconductor can often be sufficient, and sometimes even the crudest few-atom representation of TiO_2 captures the essential phenomena. This conclusion holds for both ground and low-energy excited chromophore states. However, the size of the chromophore-semiconductor interaction region increases with energy. A chromophore-metal interaction should also require much more extended representations.

Most of the reviewed work uses an atomistic description of the interface that gives the most basic and intuitive view of the phenomena from the chemist's perspective. Although atomistic models are particularly valuable for detailed studies of specific systems, general trends are captured better with simpler, more phenomenological models, some of which we include in the discussion of the electron-injection dynamics above. These simpler Hamiltonians can be analyzed by more rigorous means.

The atomistic modeling of the chromophore systems indicates that both purely organic and transition-metal-based chromophores have π^* -electronic excited states, and the electron-injection mechanisms do not strongly depend on the chromophore type. The differences between transition-metal and organic chromophores can be seen in the photoexcited-state relaxation that occurs within the chromophore and competes with the injection. Although the larger, purely organic dyes have a wider range of vibrational modes that can dissipate the electronic energy, transition metals create additional relaxation mechanisms, such as the intersystem crossing from singlet to triplet states. The vibrational modes of transition-metal chromophores couple to the electronic states more strongly because the photoexcitation involves metal-to-ligand ET and generates polar excited states. The energy of the photoexcited state can be controlled within a wide range, relative to the TiO_2 CB edge, by altering the following chromophore characteristics: the size of the π -electron system, the substituents, the presence of electronegative atoms such as oxygens, and in the case of transition-metal-based chromophores, the choice of the transition metal.

The great diversity of TiO_2 surfaces and surface defects generates a broad distribution of individual electron-injection events. Even on perfect surfaces, fluctuations in surface structure and chromophore-binding patterns significantly modulate ET times. Surface termination, the presence of solvent, and other factors further broaden the ET event distribution, generating a rich and complex picture. In every system, subsets of faster and slower ET events always exist that can occur by both direct quantum-mechanical tunneling and quasi-classical crossover through a transition state.

Most chromophores, even the simplest ones, can bind to the semiconductor by a variety of motifs, involving one or more chemical groups attached to single- or multiple-surface atoms. The type and length of the chromophore-semiconductor bridge determine the extent of dye-semiconductor-state mixing, the delocalization of the photoexcited state onto TiO_2 , the fraction of ET that occurs by direct photoexcitation into the CB, and the ET time. Although the traditional sequential picture, in which the photoexcitation is localized on the dye and is followed by the interfacial

ET, holds for long bridges and weak chromophore-semiconductor coupling, it changes with a short bridge. When the coupling is strong, the electronic wave functions of the chromophore spill onto the semiconductor and create a common chromophore-semiconductor electronic system. As a result, a significant portion of ET occurs during the photoexcitation.

The position of the chromophore excited-state energy relative to the TiO_2 CB substantially influences the ET rate and the yield in relation to relaxation processes. As the chromophore state enters deeper into the CB, both rate and yield increase, regardless of the ET mechanism, strength of the coupling, or other factors. Remarkably, fast injection is possible even close to the bottom of the CB, provided that the chromophore-semiconductor coupling is sufficiently strong. This fact carries important implications for photovoltaic and related applications because injection into the edge of the CB minimizes energy losses.

Real-time modeling of electron-vibrational dynamics is particularly valuable for understanding the interfacial electron injection because it occurs on ultrafast timescales and shows a variety of individual injection events with well-defined dynamical features that cannot be made apparent by an average rate description. Such simulations are rare, but computationally demanding state-of-the-art techniques for the dynamics simulations are currently being developed by several groups throughout the world. As the research progresses, larger systems and longer timescales will become accessible, allowing one to probe more examples and finer details of the interfacial ET and to study different surfaces, surface defects, bridges, temperature, and solvent dependence. One can anticipate that other important aspects of the interfacial ET, including the back-transfer from the surface onto the dye and the delocalization of the electron from the surface into the bulk, will be addressed by real-time dynamics simulations in the near future.

SUMMARY POINTS

1. The electron injection across the chromophore- TiO_2 interface provides an excellent model for studying the fundamental issues that arise when localized molecular species interact with periodic bulk materials. In the presence of strong chromophore- TiO_2 coupling, a combined system has to be considered explicitly, but a relatively small representation of TiO_2 is typically sufficient. Weak-coupling can be treated as a perturbation to the isolated components.
2. The ultrafast photoinduced electron injection can be understood fully only through time-resolved measurements and simulations. These techniques reveal the dynamic features that time-independent experiments and theories cannot make apparent.
3. NAMD provides an excellent tool for modeling the ET of specific systems in real time and at the atomic level of detail. Simplified representations of the interface make it possible to investigate general trends.

2. Presents many useful insights relating ET processes in purely molecular species to those in molecules inserted between solids.

4. The variety of TiO₂ surfaces, surface defects, types of chromophores, and chromophore-semiconductor binding regimes creates a great range of electron-injection events. The average behavior, however, is relatively independent of these specifics and can be predicted from a small number of concepts, such as the strength of the chromophore-semiconductor coupling, the density of semiconductor states, and alternative relaxation mechanisms.
5. Depending on the strength of the chromophore-semiconductor coupling, both adiabatic and NA ET are possible. With strong coupling, the injection proceeds primarily adiabatically into localized surface states that can be located at the edge of the TiO₂ CB. Strong enough coupling can even make ET take place during the optical excitation. The weak-coupling regime occurs if the bridge breaks direct conjugation between the chromophore and the TiO₂. In such cases, ET proceeds nonadiabatically by hopping from a localized chromophore state into a delocalized TiO₂ state. The transfer rate then depends on the density of TiO₂ states and can be described by perturbation theory (e.g., the Fermi golden rule).
6. Molecular and semiconductor vibrations play many roles in the interfacial injection dynamics. They create disorder and a broad distribution of photoexcited states, drive both adiabatic and NA ET, modulate the state localizations and donor-acceptor coupling, and are responsible for the electron-vibrational relaxation.
7. Future theoretical work in this field should address the fate of the injected electron, including electron delocalization from the surface to the bulk, energy relaxation, return to the surface, trapping, and recombination.

ACKNOWLEDGMENTS

We are indebted to many experimentalist and theoretician colleagues for fruitful and illuminating discussions, particularly to Tim Lian, Arthur Nozik, Frank Willig, Josef Wachtveitl, Victor Batista, Haobin Wang, Michael Thoss, and Volkhard May. The research was supported by NSF CAREER Award CHE-0094012, DOE Award DE-FG02-05ER15755, and ACS PRF Awards 150393 and 41436-AC6.

LITERATURE CITED

1. Nitzan A, Ratner MA. 2003. Electron transport in molecular wire junctions. *Science* 300:1384–89
2. Nitzan A. 2001. **Electron transmission through molecules and molecular interfaces.** *Annu. Rev. Phys. Chem.* 52:681–750
3. Klare JE, Tulevski GS, Sugo K, de Picciotto A, White KA, Nuckolls C. 2003. Cruciform π -systems for molecular electronics applications. *J. Am. Chem. Soc.* 125:6030–31

4. Yasutomi S, Morita T, Imanishi Y, Kimura S. 2004. A molecular photodiode system that can switch photocurrent direction. *Science* 304:1944-47
5. Zhu XY. 2004. Charge transport at metal-molecule interfaces: a spectroscopic view. *J. Phys. Chem. B* 108:8778-93
6. Fan FF, Yao Y, Cai L, Cheng L, Tour JM, Bard AJ. 2004. Structure-dependent charge transport and storage in self-assembled monolayers of compounds of interest in molecular electronics: effects of tip material, headgroup, and surface concentration. *J. Am. Chem. Soc.* 126:4035-42
7. Seminario JM. 2005. Molecular electronics: approaching reality. *Nat. Mater.* 4:111-13
8. Lewis NS. 2001. Frontiers of research in photoelectrochemical solar energy conversion. *J. Electroanal. Chem.* 508:1-10
9. Zhao W, Ma WH, Chen CC, Zhao JC, Shuai ZG. 2004. Efficient degradation of toxic organic pollutants with Ni₂O₃/TiO₂-xBx under visible irradiation. *J. Am. Chem. Soc.* 126:4782-83
10. Hirakawa T, Whitesell JK, Fox MA. 2004. Effect of temperature and pressure in the photocatalytic oxidation of n-octanol on partially desilanized hydrophobic TiO₂ suspended in aerated supercritical CO₂. *J. Phys. Chem. B* 108:10213-18
11. Cozzoli PD, Fanizza E, Comparelli R, Curri ML, Agostiana A, Laub D. 2004. Role of metal nanoparticles in TiO₂/Ag nanocomposite-based microheterogeneous photocatalysis. *J. Phys. Chem. B* 108:9623-30
12. Ho W, Yu JC, Lin J, Yu J, Li P. 2004. Preparation and photocatalytic behavior of MoS₂ and WS₂ nanocluster sensitized TiO₂. *Langmuir* 20:5865-69
13. Liu D, Hug GL, Kamat PV. 1995. Photochemistry on surfaces: intermolecular energy and electron transfer processes between excited Ru(bpy)₃²⁺ and H-aggregates of Cresyl Violet on SiO₂ and SnO₂ colloids. *J. Phys. Chem.* 99:16768-75
14. **Oregan B, Grätzel M. 1991. A low-cost, high-efficiency solar-cell based on dye-sensitized colloidal TiO₂ films. *Nature* 353:737-40**
15. Biju V, Micic M, Hu DH, Lu HP. 2004. Intermittent single-molecule interfacial electron transfer dynamics. *J. Am. Chem. Soc.* 126:9374-81
16. Tributsch H. 2004. Dye sensitization solar cells: a critical assessment of the learning curve. *Coord. Chem. Rev.* 248:1511-30
17. Anderson NA, Lian TQ. 2005. Ultrafast electron transfer at the molecule-semiconductor nanoparticle interface. *Annu. Rev. Phys. Chem.* 56:491-519
18. Watson DF, Meyer GJ. 2005. Electron injection at dye-sensitized semiconductor electrodes. *Annu. Rev. Phys. Chem.* 56:119-56
19. Arango AC, Johnson LR, Bliznyuk VN, Schlesinger Z, Carter SA, Horhold HH. 2001. Efficient titanium oxide/conjugated polymer photovoltaics for solar energy conversion. *Adv. Mater.* 12:1689-92
20. Anderson NA, Hao EC, Ai X, Hastings G, Lian TQ. 2001. Ultrafast and long-lived photoinduced charge separation in MEH-PPV/nanoporous semiconductor thin film composites. *Chem. Phys. Lett.* 347:304-10
21. Ravirajan P, Haque SA, Poplavskyy D, Durrant JR, Bradley DDC, Nelson J. 2004. Nanoporous TiO₂ solar cells sensitised with a fluorene-thiophene copolymer. *Thin Solid Films* 451-452:624-29

14. Introduced the first high-efficiency dye-sensitized semiconductor solar cell.

22. Loneragan M. 2004. Charge transport at conjugated polymer-inorganic semiconductor and conjugated polymer-metal interfaces. *Annu. Rev. Phys. Chem.* 55:257-98
23. Kucur E, Reigler J, Urban GA, Nann T. 2004. Charge transfer mechanism in hybrid bulk heterojunction composites. *J. Chem. Phys.* 120:1500-5
24. Greens W, Martens T, Poortmans J, Aernouts T, Manca J, et al. 2004. Modelling the short-circuit current of polymer bulk heterojunction solar cells. *Thin Solid Films* 451-452:498-502
25. Nozik AJ. 2001. Spectroscopy and hot electron relaxation dynamics in semiconductor quantum wells and quantum dots. *Annu. Rev. Phys. Chem.* 52:193-231
26. Schaller RD, Klimov VI. 2004. High efficiency carrier multiplication in PbSe nanocrystals: implications for solar energy conversion. *Phys. Rev. Lett.* 92:186601-4
27. Scharber MC, Mühlbacher D, Koppe M, Denk P, Waldauf C, et al. 2006. Design rules for donors in bulk-heterojunction solar cells: towards 10% energy-conversion efficiency. *Adv. Mater.* 18:789-94
28. Segura JL, Martin N, Guldi DM. 2005. Materials for organic solar cells: the C_{60}/π -conjugated oligomer approach. *Chem. Soc. Rev.* 56:31-47
29. Kymakis E, Amaratunga GAJ. 2002. Single-wall carbon nanotube/conjugated polymer photovoltaic devices. *App. Phys. Lett.* 80:112-14
30. Liu G, Klein A, Thissen A, Jaegermann W. 2003. Electronic properties and interface characterization of phthalocyanine and Ru-polypyridine dyes on TiO_2 surface. *Surf. Sci.* 539:37-48
31. Tachibana Y, Moser JE, Grätzel M, Klug DR, Durrant JR. 1996. Subpicosecond interfacial charge separation in dye-sensitized nanocrystalline titanium dioxide films. *J. Phys. Chem. B* 100:20056-62
32. Tachibana Y, Haque SA, Mercer IP, Moser JE, Klug DR, Durrant JR. 2001. Modulation of the rate of electron injection in dye-sensitized nanocrystalline TiO_2 films by externally applied bias. *J. Phys. Chem. B* 105:7424-31
33. Liu Y, Dadap JL, Zimdars D, Eisenthal KB. 1999. Study of interfacial charge-transfer complex on TiO_2 particles in aqueous suspension by second-harmonic generation. *J. Phys. Chem. B* 103:2480-86
34. Ramakrishna G, Ghosh HN, Singh AK, Palit DK, Mittal JP. 2001. Dynamics of back-electron transfer processes of strongly coupled triphenyl methane dyes adsorbed on TiO_2 nanoparticle surface as studied by fast and ultrafast visible spectroscopy. *J. Phys. Chem. B* 105:12786-96
35. Kallioinen J, Benko G, Sundstrom V, Korppi-Tommola JEI, Yartsev AP. 2002. Electron transfer from the singlet and triplet excited states of $Ru(dcbpy)_2(NCS)_2$ into nanocrystalline TiO_2 thin films. *J. Phys. Chem. B* 106:4396-404
36. Piotrowiak P, Galoppini E, Wei Q, Meyer GJ, Wiewior R. 2003. Subpicosecond photoinduced charge injection from molecular tripods into mesoporous TiO_2 over the distance of 24 angstroms. *J. Am. Chem. Soc.* 125:5278-79
37. Furube A, Katoh R, Hara K, Sato T, Murata S, et al. 2005. Lithium ion effect on electron injection from a photoexcited coumarin derivative into a TiO_2 nanocrystalline film investigated by visible-to-IR ultrafast spectroscopy. *J. Phys. Chem. B* 109:16406-14

38. Hannappel T, Burfeindt B, Storck W, Willig F. 1997. Measurement of ultrafast photoinduced electron transfer from chemically anchored Ru-dye molecules into empty electronic states in a colloidal anatase TiO₂ film. *J. Phys. Chem. B* 101:6799–802
39. Willig F, Zimmermann C, Ramakrishna S, Storck W. 2000. Ultrafast dynamics of light-induced electron injection from amolecular donor into the wide conduction band of a semiconductor as acceptor. *Electrochim. Acta* 45:4565–75
40. Ramakrishna S, Willig F. 2000. Pump-probe spectroscopy of ultrafast electron injection from the excited state of an anchored chromophore to a semiconductor surface in UHV: a theoretical model. *J. Phys. Chem. B* 104:68–77
41. Zimmermann C, Willig F, Ramakrishna S, Burfeindt B, Pettinger B, et al. 2001. Experimental fingerprints of vibrational wave-packet motion during ultrafast heterogeneous electron transfer. *J. Phys. Chem. B* 105:9245–53
42. Ramakrishna S, Willig F, May V, Knorr A. 2003. Femtosecond spectroscopy of heterogeneous electron transfer: extraction of excited-state population dynamics from pump-probe signals. *J. Phys. Chem. B* 107:607–11
43. Ramakrishna S, Willig F, Knorr A. 2004. Photoinduced bulk-surface dynamics: time resolved two photon photoemission signals at semiconductor surfaces. *Surf. Sci.* 558:159–73
44. Gundlach L, Felber S, Storck W, Galoppini E, Wei Q, Willig F. 2005. Femtosecond two-photon photoemission probing electron injection from the excited singlet state of perylene attached to a long rigid tripod anchor-cum-spacer on rutile TiO₂(110). *Res. Chem. Intermed.* 31:39–46
45. Persson P, Lundqvist MJ, Ernstorfer R, Goddard WA, Willig F. 2006. Quantum chemical calculations of the influence of anchor-cum-spacer groups on femtosecond electron transfer times in dye-sensitized semiconductor nanocrystals. *J. Chem. Theor. Comp.* 2:441–51
46. Ghosh HN, Asbury JB, Lian TQ. 1998. Direct observation of ultrafast electron injection from Coumarin 343 to TiO₂ nanoparticles by femtosecond infrared spectroscopy. *J. Phys. Chem. B* 102:6482–86
47. Asbury JB, Ellingson RJ, Ghosh HN, Ferrere S, Nozik AJ, Lian TQ. 1999. Femtosecond IR study of excited-state relaxation and electron-injection dynamics of Ru(dcbpy)₂(NCS)₂ in solution and on nanocrystalline TiO₂ and Al₂O₃ thin films. *J. Phys. Chem. B* 103:3110–19
48. Wang YQ, Asbury JB, Lian TQ. 2000. Ultrafast excited-state dynamics of Re(Co)₃Cl(dcbpy) in solution and on nanocrystalline TiO₂ and ZrO₂ thin films. *J. Phys. Chem. A* 104:4291–99
49. Asbury JB, Hao E, Wang Y, Lian T. 2000. Bridge length-dependent ultrafast electron transfer from Re polypyridyl complexes to nanocrystalline TiO₂ thin films studied by femtosecond infrared spectroscopy. *J. Phys. Chem. B* 104:11957–64
50. Asbury JB, Hao EC, Wang YQ, Ghosh HN, Lian TQ. 2001. Ultrafast electron transfer dynamics from molecular adsorbates to semiconductor nanocrystalline thin films. *J. Phys. Chem. B* 105:4545–57

50. Commonly cited feature article that gives an overview of time-resolved measurements of the photoinduced interfacial ET.

51. Hao E, Anderson NA, Asbury JB, Lian T. 2002. Effect of trap states on interfacial electron transfer between molecular absorbers and semiconductor nanoparticles. *J. Phys. Chem. B* 106:10191-98
52. Anderson NA, Ai X, Lian T. 2003. Electron injection dynamics from Ru polypyridyl complexes to ZnO nanocrystalline thin films. *J. Phys. Chem. B* 107:14414-21
53. Asbury JB, Anderson NA, Hao E, Ai X, Lian T. 2003. Parameters affecting electron injection dynamics from ruthenium dyes to titanium dioxide nanocrystalline thin film. *J. Phys. Chem. B* 107:7376-86
54. Wang Y, Hang K, Anderson NA, Lian T. 2003. Comparison of electron transfer dynamics in molecule-to-nanoparticle and intramolecular charge transfer complexes. *J. Phys. Chem. B* 107:9434-40
55. Anderson NA, Ai X, Chen DT, Mohler DL, Lian TQ. 2003. Bridge-assisted ultrafast interfacial electron transfer to nanocrystalline SnO₂ thin films. *J. Phys. Chem. B* 107:14231-39
56. Anderson NA, Lian TQ. 2004. Ultrafast electron injection from metal polypyridyl complexes to metal-oxide nanocrystalline thin films. *Coord. Chem. Rev.* 248:1231-46
57. She CX, Anderson MA, Guo JC, Liu F, Goh WH, et al. 2005. pH-dependent electron transfer from rebipyridyl complexes to metal oxide nanocrystalline thin films. *J. Phys. Chem. B* 109:19345-55
58. Huber R, Spoerlein S, Moser JE, Grätzel M, Wachtveitl J. 2000. The role of surface states in the ultrafast photoinduced electron transfer from sensitizing dye molecules to semiconductor colloids. *J. Phys. Chem. B* 104:8995-9003
59. Huber R, Moser JE, Grätzel M, Wachtveitl J. 2002. Real-time observation of photoinduced adiabatic electron transfer in strongly coupled dye/semiconductor colloidal systems with a 6 fs time constant. *J. Phys. Chem. B* 106:6494-99
60. Schnadt J, Brühwiler PA, Patthey L, O'Shea JN, Södergren S, et al. 2002. Experimental evidence for sub-3-fs charge transfer from an aromatic adsorbate to a semiconductor. *Nature* 418:620-23
61. Ramakrishna S, Willig F, May V. 2001. Theory of ultrafast photoinduced heterogeneous electron transfer: decay of vibrational coherence into a finite electronic-vibrational quasicontinuum. *J. Chem. Phys.* 115:2743-56
62. Wang LX, May V. 2004. Laser pulse control of ultrafast heterogeneous electron transfer: a computational study. *J. Chem. Phys.* 121:8039-49
63. Wang LX, Willig F, May V. 2006. Ultrafast heterogeneous electron transfer reactions: comparative theoretical studies on time- and frequency-domain data. *J. Chem. Phys.* 124:014712
64. Thoss M, Kondov I, Wang H. 2004. Theoretical study of ultrafast heterogeneous electron transfer reactions at dye-semiconductor interfaces. *Chem. Phys.* 304:169-81
65. Kondov I, Thoss M, Wang H. 2006. Theoretical study of ultrafast heterogeneous electron transfer reactions at dye-semiconductor interfaces: Coumarin 343 at titanium oxide. *J. Phys. Chem. A* 110:1364-74

66. Rego LGC, Batista VS. 2003. Quantum dynamics simulations of interfacial electron transfer in sensitized TiO₂ semiconductors. *J. Am. Chem. Soc.* 125:7989–97
67. Abuabara SG, Rego LGC, Batista VS. 2005. Influence of thermal fluctuations on interfacial electron transfer in functionalized TiO₂ semiconductors. *J. Am. Chem. Soc.* 127:18234–42
- 68. Stier W, Prezhdo OV. 2002. Nonadiabatic molecular dynamics simulation of light-induced, electron transfer from an anchored molecular electron donor to a semiconductor acceptor. *J. Phys. Chem. B* 106:8047–54**
69. Stier W, Prezhdo OV. 2003. Thermal effects in the ultrafast photoinduced electron transfer from a molecular donor anchored to a semiconductor acceptor. *Isr. J. Chem.* 42:213–24
70. Stier W, Duncan WR, Prezhdo OV. 2003. Ab initio molecular dynamics of ultrafast electron injection from molecular donors to the TiO₂ acceptor. *SPIE Proc.* 5223:132–46
71. Stier W, Duncan WR, Prezhdo OV. 2004. Thermally assisted sub10 fs electron transfer in dye-sensitized nanocrystalline TiO₂ solar cells. *Adv. Mater.* 16:240–44
72. Duncan WR, Stier WM, Prezhdo OV. 2005. Ab initio nonadiabatic molecular dynamics of the ultrafast electron injection across the alizarin-TiO₂ interface. *J. Am. Chem. Soc.* 127:7941–51
73. Duncan WR, Prezhdo OV. 2005. Nonadiabatic molecular dynamics study of electron transfer from alizarin to the hydrated Ti⁴⁺ ion. *J. Phys. Chem. B* 109:17998–8002
74. Duncan WR, Prezhdo OV. 2005. Electronic structure and spectra of catechol and alizarin in the gas phase and attached to titanium. *J. Phys. Chem. B* 109:365–73
- 75. Craig CF, Duncan WR, Prezhdo OV. 2005. Trajectory surface hopping in the time-dependent Kohn-Sham approach for electron-nuclear dynamics. *Phys. Rev. Lett.* 95:163001**
76. Hoffmann R. 1988. *Solids and Surfaces: A Chemist's View of Bonding in Extended Structures*. New York:VCH
77. Malliaras G, Friend R. 2005. An organic electronics primer. *Phys. Today* 5:53–58
78. Linsebigler AL, Lu G, Yates JTJ. 1995. Photocatalysis on TiO₂ surfaces: principles, mechanisms, and selected results. *Chem. Rev.* 95:735–58
79. Diebold U. 2003. **The surface science of titanium dioxide.** *Surf. Sci. Rep.* 48:53–229
80. Shapovalov V, Wang Y, Truong TN. 2003. Theoretical analysis of the electronic spectra of water absorbed on the rutile TiO₂ (110) and MgO (100) surfaces. *Chem. Phys. Lett.* 375:321–27
81. Zhang Z, Fenter P, Cheng L, Sturchio NC, Bedzyk MJ, et al. 2004. Ion adsorption at the rutile-water interface: linking molecular and macroscopic properties. *Langmuir* 20:4954–69
82. Moser J, Gratzel M. 1983. Light-induced electron-transfer in colloidal semiconductor dispersions: single vs dielectronic reduction of acceptors by conduction-band electrons. *J. Am. Chem. Soc.* 105:6547–55

68. First time-domain ab initio study of the photoinduced interfacial ET.

75. Combined the most popular approaches to NA dynamics and electronic structure, allowing one to model excitation dynamics in real time in many condensed-phase systems.

76. Presents a chemist's view of the solid-state structure.

77. Presents a physicist's account of conjugated molecular systems.

79. Discusses the structure of many different TiO₂ surfaces and molecular-binding modes.

86. Covers a wide range of topics on ET at semiconductor interfaces, including the photoinduced injection from sensitizer dyes.

99. Introduction to advanced electronic-structure theory.

100. A monograph on DFT written for chemists.

83. Gregg BA. 2004. Interfacial processes in the dye-sensitized solar cell. *Coord. Chem. Rev.* 248:1215–24
84. Argazzi R, Iha NYM, Zabri H, Odobel F, Bignozzi CA. 2004. Design of molecular dyes for application in photoelectrochemical and electrochromic devices based on nanocrystalline metal oxide semiconductors. *Coord. Chem. Rev.* 248:1299–316
85. Hagfeldt A, Grätzel M. 2000. Molecular photovoltaics. *Acc. Chem. Res.* 33:269–77
- 86. Memming R. 2001. *Semiconductor Electrochemistry*. Weinheim, Ger.: Wiley-VCH**
87. Katoh R, Furube A, Barzykin AV, Arakawa H, Tachiya M. 2004. Kinetics and mechanism of electron injection and charge recombination in dye-sensitized nanocrystalline semiconductors. *Coord. Chem. Rev.* 248:1195–213
88. Langel W. 2002. Car-Parrinello simulation of H₂O dissociation on rutile. *Surf. Sci.* 496:141–50
89. Menetrey M, Markovits A, Minot C. 2003. Reactivity of a reduced metal oxide surface: hydrogen, water and carbon monoxide adsorption on oxygen defective rutile TiO₂(110). *Surf. Sci.* 524:49–62
90. Kornherr A, Vogtenhuber D, Ruckebauer M, Podlousky R, Zifferer G. 2004. Multilayer adsorption of water at a rutile TiO₂(110) surface: towards a realistic modeling by molecular dynamics. *J. Chem. Phys.* 121:3722–26
91. Bandura AV, Sykes DG, Shapovalov V, Troung TN, Kubicki JD, Evarestov RA. 2004. Adsorption of water on the TiO₂ (rutile) (110) surface: a comparison of periodic and embedded cluster calculations. *J. Phys. Chem. B* 108:7844–53
92. Redfern PC, Zapol P, Curtiss LA, Rajh T, Thurnauer MC. 2003. Computational studies of catechol and water interactions with titanium oxide nanoparticles. *J. Phys. Chem. B* 107:11419–27
93. Ahdjoudj J, Minot C. 1997. A theoretical study of HCO₂H adsorption on TiO₂(110). *Catal. Lett.* 46:83–91
94. Wang LQ, Ferris KF, Schultz AN, Baer DR, Engelhard MH. 1997. Interactions of HCOOH with stoichiometric and defective TiO₂(110) surfaces. *Surf. Sci.* 380:352–64
95. Vittadini A, Selloni A, Rotzinger FP, Grätzel M. 2000. Formic acid adsorption on dry and hydrated TiO₂ anatase (101) surfaces by DFT calculations. *J. Phys. Chem. B* 104:1300–6
96. Persson P, Bergström R, Lunell S. 2000. Quantum chemical study of photoinjection processes in dye-sensitized TiO₂ nanoparticles. *J. Phys. Chem. B* 104:10348–51
97. Hara K, Wang ZS, Sato T, Furube A, Katoh R, et al. 2005. Oligothiophene-containing coumarin dyes for efficient dye-sensitized solar cells. *J. Phys. Chem. B* 109:15476–82
98. Kondov I, Thoss M, Wang H. 2006. Computational study of titanium (IV) complexes with organic chromophores. *Int. J. Quantum Chem.* 106:1291–303
- 99. Szabo A, Ostlund NS. 1996. *Modern Quantum Chemistry*. Canada: Dover**
- 100. Parr RG, Yang W. 1989. *Density Functional Theory of Atoms and Molecules*. Oxford, UK: Oxford Univ. Press**

101. Persson P, Lunell S. 2000. Binding of bi-isonicotinic acid to anatase TiO₂ (101). *Sol. Energy Mater. Sol. Cells* 63:139–48
102. Odelius M, Persson P, Lunell S. 2003. Bi-isonicotinic acid on rutile (110): calculated molecular and electronic structure. *Surf. Sci.* 529:47–58
103. Patthey L, Rensmo H, Persson P, Westermark K, Vayssieres L, et al. 1999. Adsorption of bi-isonicotinic acid on rutile TiO₂(110). *J. Chem. Phys.* 110:5913–18
104. Zabri H, Gillaizeau I, Bignozzi CA, Caramori S, Charlot MF, et al. 2003. Synthesis and comprehensive characterizations of new *cis*-RuL₂ × 2 (X = Cl, Cn, and NCS) sensitizers for nanocrystalline TiO₂ solar cell using bis-phosphonated bipyridine ligands (L). *Inorg. Chem.* 42:6655–66
105. Schnadt J, Henningsson A, Andersson MP, Karlsson PG, Uvdal P, et al. 2004. Adsorption and charge-transfer study of bi-isonicotinic acid on in situ-grown anatase TiO₂ nanoparticles. *J. Phys. Chem. B* 108:3114–22
106. Persson P, Lundqvist MJ. 2005. Calculated structural and electronic interactions of the ruthenium dye N3 with a titanium dioxide nanocrystal. *J. Phys. Chem. B* 109:11918–24
107. Ishiwaki T, Inoue H, Makishima A. 2000. Electronic structures of quinizarin complexed with TiO₂ clusters. *J. Mater. Sci.* 35:1669–74
108. Karabunarliev S, Baumgarten M, Müllen K. 1998. Crossover to an even-parity lowest excited singlet in large oligorylenes: a theoretical study. *J. Phys. Chem. B.* 102:7029–34
109. Karabunarliev S, Gherghel L, Koch KH, Baumgarten M. 1994. Structure and optical-absorption of oligorylenes upon doping. *Chem. Phys.* 189:53–65
110. Viruelamartin R, Viruelamartin PM, Orti E. 1992. Theoretical determination of the geometric and electronic-structures of oligorylenes and poli(perinaphthalene). *J. Chem. Phys.* 97:8470–80
111. Rensmo H, Sodergren S, Patthey L, Westermark K, Vayssieres L, et al. 1997. The electronic structure of the *cis*-bis(4,4'-dicarboxy-2,2'-bipyridine)-bis(isothiocyanato) ruthenium(II) complex and its ligand 2,2'-bipyridyl-4,4'-dicarboxylic acid studied with electron spectroscopy. *Chem. Phys. Lett.* 274:51–57
112. Aiga F, Tada T. 2003. Molecular and electronic structures of black dye; an efficient sensitizing dye for nanocrystalline TiO₂ solar cells. *J. Mol. Struct.* 658:25–32
113. Nazeeruddin MK, Zakeeruddin SM, Humphry-Baker R, Gorelsky SI, Lever ABP, Grätzel M. 2000. Synthesis, spectroscopic and a zindo study of *cis*- and *trans*-(x-2)bis(4,4'-dicarboxylic acid-2,2'-bipyridine)ruthenium(II) complexes (X = Cl⁻, H₂O, NCS⁻). *Coord. Chem. Rev.* 208:213–25
114. Srikanth K, Marathe VR, Mishra MK. 2002. Role of electronic structure of ruthenium polypyridyl dyes in the photoconversion efficiency of dye-sensitized solar cells: semiempirical investigation. *Int. J. Quantum Chem.* 89:535–49
115. De Angelis F, Fantacci S, Selloni A. 2004. Time-dependent density functional theory study of the absorption spectrum of [Ru(4,4'-COOH-2,2'-bpy)₂(NCS)₂] in water solution: influence of the pH. *Chem. Phys. Lett.* 389:204–8

116. Gives foundations of various approximations used in simulations of excitation dynamics in condensed phase.

117. A pedagogical introduction to NAMD.

124. Overview of the quantized Hamilton dynamics method that systematically incorporates quantum nuclear effects into classical molecular dynamics.

128. A review of time-dependent DFT from one of its founders.

116. Tully JC. 1998. *Classical and Quantum Dynamics in Condensed Phase Simulations*. Singapore: World Sci.
117. Drukker K. 1999. Basics of surface hopping in mixed quantum/classical simulations. *J. Comp. Phys.* 153:225–72
118. Worth GA, Cederbaum LS. 2004. Beyond Born-Oppenheimer: molecular dynamics through a conical intersection. *Annu. Rev. Phys. Chem.* 55:127–58
119. Jasper AW, Nangia S, Zhu CY, Truhlar DG. 2006. Non-Born-Oppenheimer molecular dynamics. *Acc. Chem. Res.* 39:101–8
120. Prezhdo OV, Rossky PJ. 1997. Mean field molecular dynamics with surface hopping. *J. Chem. Phys.* 107:825–34
121. Prezhdo OV. 1999. Mean field approximation for the stochastic Schrodinger equation. *J. Chem. Phys.* 111:8366–77
122. Prezhdo OV, Pereverzev YV. 2000. Quantized Hamilton dynamics. *J. Chem. Phys.* 113:6557–65
123. Prezhdo OV, Brooksby C. 2001. Quantum backreaction through the Bohmian particle. *Phys. Rev. Lett.* 86:3215–19
124. Prezhdo OV. 2005. Quantized Hamilton dynamics. *Theor. Chem. Acc.* 116: 206–218
125. Kresse G, Hafner J. 1994. Ab initio molecular-dynamics simulation of the liquid-metal wamorphous-semiconductor transition in germanium. *Phys. Rev. B* 49:14251–69
126. Kresse G, Furthmüller J. 1996. Efficiency of ab-initio total energy calculations for metals and semiconductors using a plane-wave basis set. *Comput. Mater. Sci.* 6:15–50
127. Kresse G, Furthmüller J. 1996. Efficient iterative schemes for ab initio total-energy calculations using a plane-wave basis set. *Phys. Rev. B* 54:11169–86
128. Marques MAL, Gross EKV. 2004. Time-dependent density functional theory. *Annu. Rev. Phys. Chem.* 55:427–55
129. Hammes-Schiffer S, Tully JC. 1994. Proton-transfer in solution: molecular-dynamics with quantum transitions. *J. Chem. Phys.* 101:4657–67
130. Leforestier C, Bisseling RH, Cerjan C, Feit MD, Friesner R, et al. 1991. A comparison of different propagation schemes for the time-dependent Schrodinger-equation. *J. Comp. Phys.* 94:59–80
131. Toben L, Gundlach L, Ernstorfer R, Eichberger R, Hannappel T, et al. 2005. Femtosecond transfer dynamics of photogenerated electrons at a surface resonance of reconstructed InP(100). *Phys. Rev. Lett.* 94:067601



Contents

Frontispiece	
<i>C. Bradley Moore</i>	xvi
A Spectroscopist's View of Energy States, Energy Transfers, and Chemical Reactions	
<i>C. Bradley Moore</i>	1
Stochastic Simulation of Chemical Kinetics	
<i>Daniel T. Gillespie</i>	35
Protein-Folding Dynamics: Overview of Molecular Simulation Techniques	
<i>Harold A. Scheraga, Mey Khalili, and Adam Liwo</i>	57
Density-Functional Theory for Complex Fluids	
<i>Jianzhong Wu and Zhidong Li</i>	85
Phosphorylation Energy Hypothesis: Open Chemical Systems and Their Biological Functions	
<i>Hong Qian</i>	113
Theoretical Studies of Photoinduced Electron Transfer in Dye-Sensitized TiO ₂	
<i>Walter R. Duncan and Oleg V. Prezhdo</i>	143
Nanoscale Fracture Mechanics	
<i>Steven L. Mielke, Ted Belytschko, and George C. Schatz</i>	185
Modeling Self-Assembly and Phase Behavior in Complex Mixtures	
<i>Anna C. Balazs</i>	211
Theory of Structural Glasses and Supercooled Liquids	
<i>Vassiliy Lubchenko and Peter G. Wolynes</i>	235
Localized Surface Plasmon Resonance Spectroscopy and Sensing	
<i>Katherine A. Willets and Richard P. Van Duyne</i>	267
Copper and the Prion Protein: Methods, Structures, Function, and Disease	
<i>Glenn L. Millhauser</i>	299

Aging of Organic Aerosol: Bridging the Gap Between Laboratory and Field Studies <i>Ynon Rudich, Neil M. Donahue, and Thomas F. Mentel</i>	321
Molecular Motion at Soft and Hard Interfaces: From Phospholipid Bilayers to Polymers and Lubricants <i>Sung Chul Bae and Steve Granick</i>	353
Molecular Architectonic on Metal Surfaces <i>Johannes V. Barth</i>	375
Highly Fluorescent Noble-Metal Quantum Dots <i>Jie Zheng, Philip R. Nicovich, and Robert M. Dickson</i>	409
State-to-State Dynamics of Elementary Bimolecular Reactions <i>Xueming Yang</i>	433
Femtosecond Stimulated Raman Spectroscopy <i>Philipp Kukura, David W. McCamant, and Richard A. Mathies</i>	461
Single-Molecule Probing of Adsorption and Diffusion on Silica Surfaces <i>Mary J. Wirth and Michael A. Legg</i>	489
Intermolecular Interactions in Biomolecular Systems Examined by Mass Spectrometry <i>Thomas Wytenbach and Michael T. Bowers</i>	511
Measurement of Single-Molecule Conductance <i>Fang Chen, Joshua Hibath, Zhibeng Huang, Xiulan Li, and N.J. Tao</i>	535
Structure and Dynamics of Conjugated Polymers in Liquid Crystalline Solvents <i>P.F. Barbara, W.-S. Chang, S. Link, G.D. Scholes, and Arun Yethiraj</i>	565
Gas-Phase Spectroscopy of Biomolecular Building Blocks <i>Mattanjah S. de Vries and Pavel Hobza</i>	585
Isomerization Through Conical Intersections <i>Benjamin G. Levine and Todd J. Martínez</i>	613
Spectral and Dynamical Properties of Multiexcitons in Semiconductor Nanocrystals <i>Victor I. Klimov</i>	635
Molecular Motors: A Theorist's Perspective <i>Anatoly B. Kolomeisky and Michael E. Fisher</i>	675
Bending Mechanics and Molecular Organization in Biological Membranes <i>Jay T. Groves</i>	697
Exciton Photophysics of Carbon Nanotubes <i>Mildred S. Dresselhaus, Gene Dresselhaus, Riichiro Saito, and Ado Jorio</i>	719